

# On the thickness of the skin layer for screening of the leptonic charge of a body

B. V. Martemyanov

*Institute of Theoretical & Experimental Physics, 117259 Moscow, Russia*

(Submitted 15 September 1997)

*Pis'ma Zh. Éksp. Teor. Fiz.* **66**, No. 8, 513–514 (25 October 1997)

The problem of the skin layer for the screening of the leptonic charge of a body by condensed bosons is considered. © 1997 American Institute of Physics. [S0021-3640(97)00120-5]

PACS numbers: 03.75.Fi, 72.30.+q

The authors of Refs. 1–3 have considered the possible existence of a leptonic (electronic) photon for a range of values of the leptonic charge. They discussed the possibility that light stable scalar bosons, unlike fermions (antineutrinos), may neutralize the electron repulsion in condensed bodies. For this purpose in Ref. 3 the problem of the skin layer for bosons was compared with that for fermions. According to Ref. 3 the thickness of the skin is of the order of the Compton wavelength of the boson. We will argue that this statement cannot be correct in all cases. In fact, this thickness should depend on the leptonic coupling constant ( $\alpha_l$ ), the electron density ( $n$ ) in the condensed body, and the mass ( $m$ ) of the boson in a combination which we are going to discuss in this paper.

Following Ref. 3, let us consider condensed bosons near the surface of a solid body. They are described by the field  $\Phi$ . This field,  $\Phi = e^{-iEt}\phi$ , and the leptostatic potential  $A_0$  are solutions of the field equations

$$(E + gA_0)^2 \phi + \nabla^2 \phi = m^2 \phi, \quad (1)$$

$$-\nabla^2 A_0 = gn - g2(E + gA_0)\phi^2. \quad (2)$$

Here  $g = \sqrt{4\pi\alpha_l}$ , and  $E$  is the lowest energy of the bosons. Let  $A_0 = 0$  inside the body, so that  $A_0$  outside the body will represent the jump of the potential across the skin layer. In what follows we will consider two cases: nonrelativistic and relativistic approximations for Eqs. (1) and (2). As we will see, the approximation depends on the value of the dimensionless parameter  $\gamma = (\alpha_l n / m^3)^{1/3}$ .

First, let us consider the case when  $gA_0 \ll m$ ,  $E = m + \delta E$ ,  $\delta E \ll m$  (nonrelativistic approximation). Then we get from Eq. (1)

$$\delta E \phi \approx \left( -\frac{\nabla^2}{2m} - gA_0 \right) \phi \quad (3)$$

and from Eq. (2)

$$-\nabla^2 A_0 \approx gn - g2m\phi^2. \quad (4)$$

Using only dimensional considerations we can determine from the above equations the dependence of the thickness of the transition region  $d$  and the jump of the potential energy of the boson  $gA_0$  on the parameters of the model:

$$d \sim (\alpha_l n m)^{-1/4}, \quad gA_0 \sim (\alpha_l n / m)^{1/2}. \quad (5)$$

Our approximation  $gA_0/m \ll 1$  means that  $\gamma = (\alpha_l n / m^3)^{1/3} \ll 1$ . Then,  $1/md \sim (\alpha_l n / m^3)^{1/4}$  and  $d \gg 1/m$ , contrary to Ref. 3.

Second, let us consider the case  $m \rightarrow 0$  ( $m \ll (\alpha_l n)^{1/3}$ ,  $\gamma \gg 1$ ). Neglecting  $m$  in Eqs. (1) and (2) we get the following formulas for  $d$  and  $gA_0$  (we do not consider here the problem of whether the solution exists; in one special case<sup>4</sup> the solution has been found numerically):

$$d \sim (\alpha_l n)^{-1/3} \ll 1/m, \quad gA_0 \sim (\alpha_l n)^{1/3}. \quad (6)$$

Looking at the expressions (5), (6) for  $d$  in two limiting cases, we see that  $d \sim \gamma^{1/4} (\alpha_l n)^{-1/3}$  (nonrelativistic case,  $\gamma \ll 1$ ), and therefore  $d \sim (\alpha_l n)^{-1/3}$  (relativistic case) is the largest possible value of the thickness of the skin layer for all  $m$ . Let us compare it with the critical size of the grain in the case of unscreened electrons,  $r_c \sim \alpha / \alpha_l^{1/2} n^{1/3}$  (Ref. 3):

$$d/r_c \sim \alpha_l^{1/6} / \alpha. \quad (7)$$

We see that for  $\alpha_l < 10^{-12}$  one has  $d < r_c$ , and the skin layer is stable against the ‘‘peeling’’ process.<sup>3</sup>

In conclusion, using only dimensional arguments we have estimated the thickness of the skin layer of a leptonically charged body screened by hypothetical light bosons. It seems reasonable that the thickness of the skin layer is smaller than  $(\alpha_l n)^{-1/3}$  and that ‘‘peeling’’ of the surface of the body does not occur for  $\alpha_l < 10^{-12}$ . It is clear that the problem needs further investigation from the standpoint of the existence of solutions of Eqs. (1) and (2).

The author acknowledges some stimulating discussions with L. B. Okun and critical remarks by M. B. Voloshin.

<sup>1</sup>L. B. Okun, ‘‘A remark on leptonic photons’’ [in Russian], manuscript presented at the ITEP theoretical seminar, June 1972.

<sup>2</sup>A. K. Ciftci, S. Sultansoy and S. Turkoz, Phys. Lett. B **355**, 494 (1995).

<sup>3</sup>S. I. Blinnikov, A. D. Dolgov, L. B. Okun and M. B. Voloshin, Nucl. Phys. B **458**, 52 (1996).

<sup>4</sup>J. E. Mandula, Phys. Lett. B **69**, 495 (1977).

Published in English in the original Russian journal. Edited by Steve Torstveit.

## Circular electrochromism of light in isotropic optically active media

N. I. Koroteev

*M. V. Lomonosov Moscow State University, 119899 Moscow, Russia*

(Submitted 9 September 1997)

*Pis'ma Zh. Éksp. Teor. Fiz.* **66**, No. 8, 515–520 (25 October 1997)

Circular electrochromism is predicted in liquids and gases containing unequal concentrations of mirror stereoisomers of chiral molecules. A longitudinal (quasi)static electric field increases absorption for a light wave circularly polarized in one direction and decreases the absorption for a wave circularly polarized in the opposite direction. The corresponding nonlinear susceptibility is proportional to the decay constants of the excited states and is absent in a nondissipative medium. Estimates of the magnitude of the effect are presented and show that it may well be observable experimentally. © 1997 American Institute of Physics. [S0021-3640(97)00220-X]

PACS numbers: 33.55.Ad, 78.20.Jq

1. This letter discusses a new electrooptic effect in isotropic, optically active liquids and gases belonging to the limiting symmetry class  $\infty\infty$ , i.e., liquids and gases consisting of freely rotating chiral (mirror dissymmetric) molecules or their nonracemic mixtures. The effect consists of the fact that within the light absorption bands on electric-dipole transitions of the chiral molecules under study a (quasi)static electric field can give rise to additional absorption (or differential amplification) for light waves with left (right) circular polarization. The electrostatically induced additional absorption/differential amplification coefficient for each of two circularly polarized components of a light wave is related linearly with the intensity of the applied electric field and changes sign with a change in both the direction of the field and the sign of the circular polarization of the light wave. The sign of the electrooptic effect under discussion likewise changes when each enantiomer of the constituent chiral molecules of the experimental medium is replaced by its “mirror antipode.” For this reason, the effect does not occur in racemic mixtures of chiral molecules or in optically inactive liquids and gases. Thus it is chirally specific and can be used as a basis for a new method of spectroscopy of mirror-asymmetric molecules in solutions, of which biological macromolecules are a very important class.<sup>1</sup>

2. The new electrooptic effect in optically active liquids and gases is appropriately termed circular electrochromism (CED) by analogy to ordinary circular dichroism (the difference arising between the absorption coefficients for light with right/left circular polarization as a result of the natural optical activity of the chiral molecules). Circular electrochromism supplements the electrical analog of the Faraday effect, previously discussed theoretically,<sup>2</sup> in the presence of electrical conductivity, or the linear electrooptic effect<sup>3</sup> in the presence of absorption in such media, in which an additional (besides the

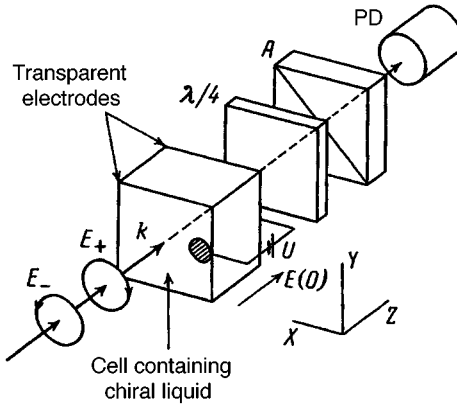


FIG. 1. Arrangement of an experiment proposed for observing circular electrochromism. A plane circularly polarized light wave with right or left circular polarization is introduced into a chiral isotropic medium in a direction along an electrostatic field applied to the medium. To detect the CED, a quarter-wave plate ( $\lambda/4$ ) and a polarization analyzer  $A$  are inserted into the beam. Detection is performed with a photodetector PD.

standard rotation due to the natural optical activity) rotation of the plane of polarization of the light arises which is proportional to the intensity of the static electric field applied to the medium. Circular electrochromism has until now been absent from among the nonlinear optical effects in chiral liquids and gases which have been observed experimentally or discussed in the literature (generation of sum and difference frequencies accompanying an electric-dipole interaction in the bulk of a medium,<sup>4-6</sup> optical rectification,<sup>3,6,7</sup> generation of the second optical harmonic,<sup>8,9</sup> generation of the sum and difference frequencies<sup>10,11</sup> on reflection from an interface, and effects which are of fourth order in the field<sup>5,6,12,13</sup>).

3. Let us consider the geometry of an experiment on the detection of CED (Fig. 1). The geometry is close to that proposed previously for observing a linear electrooptic effect in chiral liquids and gases possessing electrical conductivity<sup>2</sup> or near absorption bands.<sup>3,6</sup> Let us expand an elliptically polarized monochromatic plane light wave, introduced from the outside into the experimental optically active isotropic medium, in terms of the characteristic modes of this medium — circularly polarized plane waves:

$$\mathbf{E}(t, z) = \frac{1}{2} \mathbf{E}(\omega, z) e^{-i\omega t} + \text{c.c.} = \frac{1}{2} (E_+ \mathbf{e}_+ e^{ik_+z} + E_- \mathbf{e}_- e^{ik_-z}) e^{-i\omega t} + \text{c.c.}, \quad (1)$$

where  $\mathbf{e}_\pm = 1/\sqrt{2} (\mathbf{e}_x \pm i\mathbf{e}_y)$  are the unit right (+) and left (-) circular polarization vectors,

$$k_\pm = \frac{\omega}{c} n_\pm(\omega) \quad (2)$$

are the wave numbers of the corresponding characteristic modes, and  $n_\pm(\omega)$  are the

linear refractive indices (in the general case, complex numbers). A similar representation is also valid for a wave of nonlinear polarization engendered by the interaction of electrostatic and optical fields in the medium

$$\mathbf{P}(t, z) = \frac{1}{2} \mathbf{P}(\omega, z) e^{-i\omega t} + \text{c.c.} = \frac{1}{2} (P_+ \mathbf{e}_+ e^{ik_+z} + P_- \mathbf{e}_- e^{ik_-z}) e^{-i\omega t} + \text{c.c.} \quad (3)$$

The optimal orientation of the static field for manifestation of dichroic electroabsorption is along the  $z$  axis (see Fig.1)

$$\mathbf{E}(0) = E_0 \mathbf{e}_z. \quad (4)$$

In accordance with expression (13) from Ref. 6

$$\mathbf{P}(\omega, z) = \chi(\omega) [\mathbf{E}(\omega, z) \times \mathbf{E}(0)], \quad (5)$$

where

$$\chi(\omega) = \chi(\omega; \omega, 0) + \chi^*(-\omega; -\omega, 0), \quad (6)$$

$$\begin{aligned} \chi(\omega; \omega, 0) = \frac{1}{6} \{ & \chi_{xyz}^{(2)}(\omega; \omega, 0) + \chi_{yzx}^{(2)}(\omega; \omega, 0) + \chi_{zxy}^{(2)}(\omega; \omega, 0) - \chi_{xzy}^{(2)}(\omega; \omega, 0) - \chi_{zyx}^{(2)} \\ & \times (\omega; \omega, 0) - \chi_{yxz}^{(2)}(\omega; \omega, 0) \} \end{aligned} \quad (6a)$$

is a pseudoscalar, which is the only nonzero invariant of the quadratic nonlinear susceptibility tensor  $\chi_{ijk}^{(2)}(\omega; \omega, 0)$  of the chiral medium.

From Eqs. (1), (3), and (5) we obtain

$$P_{\pm} = \pm i \chi(\omega) E_{\pm} E_0. \quad (7)$$

Hence it is obvious that in the presence of a longitudinal electric field the characteristic modes of the medium remain circularly polarized electromagnetic waves. The nonlinear polarization (3) and (7) gives an addition to the permittivity of the medium at the optical frequency  $\omega$ :

$$\epsilon_{\pm}(\omega, E_0) = \epsilon_{\pm}^0(\omega) \pm i 4 \pi \chi(\omega) E_0, \quad (8)$$

where  $\epsilon_{\pm}^0(\omega)$  are the permittivities of the medium for light waves with right/left circular polarizations in the absence of an electrostatic field, and correspondingly an addition to the complex refractive index

$$n_{\pm}(\omega, E_0) = \sqrt{\epsilon_{\pm}(\omega, E_0)} \approx n_{\pm}(\omega) \pm i \frac{2\pi}{n_0} \chi(\omega) E_0; \quad (9)$$

(we assume that  $|(2\pi/n_0) \chi(\omega) E_0| \ll 1$  and  $n_0 = \frac{1}{2}(n_+(\omega) + n_-(\omega))$ ). Hence and from Eq. (2) one can see that the wave numbers of both characteristic circularly polarized modes of the light field change in the presence of an electrostatic field and become complex quantities proportional to the intensity of this field

$$k_{\pm}(E_0) = k_{\pm} \pm \Delta k(E_0), \quad (10)$$

$$\Delta k(E_0) = i \frac{2\pi\omega}{n_0 c} \chi(\omega) E_0 \equiv \frac{\omega n_0}{c^2} \Delta c + i \Delta \alpha, \quad (11)$$

where

$$\Delta c \equiv \frac{1}{2} (c_+(E_0) - c_-(E_0)) \approx \frac{2\pi c}{n_0^3} E_0 \operatorname{Im} \chi \quad (12)$$

is the change in the phase velocity and

$$\Delta \alpha \equiv \frac{1}{2} (\alpha_+(\omega, E_0) - \alpha_-(\omega, E_0)) \approx \frac{2\pi\omega}{n_0 c} E_0 \operatorname{Re} \chi \quad (13)$$

is the change in the absorption coefficient for the corresponding circular components of the light field (1);  $\operatorname{Re} \chi$  and  $\operatorname{Im} \chi$  are, respectively, the real and imaginary parts of the pseudoscalar (6):  $\chi(\omega) = \operatorname{Re} \chi + i \operatorname{Im} \chi$ .

Obviously, the quantity  $\Delta c$  is responsible for the static-field-induced rotation of the major axis of the polarization ellipse of the light wave, i.e., for the electric analog of the Faraday effect<sup>2</sup> or the linear electrooptic effect.<sup>3,6</sup> The quantity  $\Delta \alpha$  describes circular electro-dichroism, which in the present case manifests as a change in the ellipticity of the light wave.

The nontrivial nature of expressions (12) and (13) lies in the fact that here the imaginary part of the nonlinear susceptibility is responsible for the phase change of the light wave and the real part is responsible for the change in the absorption/amplification of the light wave, while in ordinary nonlinear optics the real and imaginary parts of the nonlinear susceptibilities play directly opposite roles.<sup>14,15</sup>

In CED the presence of a nonzero real part in  $\chi(\omega)$  has the effect that the absorption coefficient of one of the circularly polarized components of the light field increases and the absorption for the other component correspondingly decreases (as indicated by the  $\pm$  signs in Eq. (10)).

Theoretically it can be expected that for a sufficiently high value of  $E_0$ ,

$$E_0 > E_{0,th} \approx \frac{n_0 \alpha(\omega) \lambda}{4\pi^2 |\operatorname{Re} \chi(\omega)|}, \quad (14)$$

the amplification for the latter circularly polarized component of the light field will exceed the losses, so that by introducing feedback it will be possible to realize a parametric generator of circularly polarized light excited by a static electric field. Of course, this is possible only when the threshold intensity (14) is, first, lower than the threshold of dielectric breakdown of the chiral medium and, second, high enough so that terms of higher order in  $E_0$  would change the linear electric-field dependence of the CED.

It should be noted that the CED is also possible in class 432 cubic crystals, whose quadratic optical susceptibility tensor has the same form as in chiral liquids and gases.<sup>4,16</sup>

**4.** A quantum-mechanical expression for the pseudoscalar  $\chi(\omega)$  can be obtained from the standard perturbation-theory formula<sup>17</sup> for the tensor  $\chi_{ijk}^{(2)}(\omega; \omega_1, \pm \omega_2)$  describ-

ing the summation and subtraction of the optical frequencies  $\omega_1$  and  $\omega_2$ , one frequency (for example,  $\omega_2$ ) being made to approach zero and averaging the corresponding expression over the arbitrary orientations of the chiral molecules:

$$\begin{aligned} \chi(\omega) = & -4i\omega \frac{NL^3}{3} \sum_{g,k,j} \left[ \frac{\Gamma_{kg}(1-\omega^2/\omega_{kg}^2) - \Gamma_{jg}(1-\omega^2/\omega_{jg}^2)}{(\tilde{\omega}_{kg} - \omega)(\tilde{\omega}_{jg} - \omega)(\tilde{\omega}_{kg}^* + \omega)(\omega_{jg}^* + \omega)} \right. \\ & \left. + \frac{1}{2}K' \frac{\tilde{\omega}_{kg} + \tilde{\omega}_{jg}^*}{(\tilde{\omega}_{jg}^* + \omega)(\tilde{\omega}_{kg} - \omega)\tilde{\omega}_{jg}^* \tilde{\omega}_{kg}} - \frac{1}{2}K'^* \frac{\tilde{\omega}_{kg}^* + \tilde{\omega}_{jg}}{(\tilde{\omega}_{jg} - \omega)(\tilde{\omega}_{kg}^* + \omega)\tilde{\omega}_{jg} \tilde{\omega}_{kg}^*} \right] \\ & \times (\mathbf{R}_{gk} \cdot [\mathbf{R}_{kj} \times \mathbf{R}_{jg}]). \end{aligned} \quad (15)$$

In the derivation of this formula, only terms linear in  $\Gamma_{jg}$  and  $\Gamma_{kg}$  were retained in the numerator of the first term in the summation, and the terms of second and higher order in these quantities were dropped.

Here  $g$  and  $j, k$  enumerate, respectively, the ground and excited electronic states of the chiral molecules, whose volume density is  $N$ . In the case when the medium under study consists of a nonracemic mixture of mirror enantiomers of chiral molecules with densities  $N_1$  and  $N_2$ ,  $N = N_1 - N_2$ ,  $L \approx (n^2 + 1)/3$  is a correction factor for the local field,  $\tilde{\omega}_{jg} = \omega_{jg} - i\Gamma_{jg}$  (and so on) are the complex frequencies of the  $g-j$  transitions (and so on),  $\Gamma_{jg}$  and so on are damping constants, and  $\mathbf{R}_{gj}$  and so on are the dipole moments of the corresponding transitions (in the calculation, the latter were assumed to be real quantities). The factor  $K'$  is different zero only in the case of nonradiational broadening of the excited states:<sup>17</sup>

$$K' = (\Gamma_{kj} - \Gamma_{kg} - \Gamma_{gj}) / (\tilde{\omega}_{kj} - \omega). \quad (16)$$

As one can see from Eq. (15), the susceptibility  $\chi(\omega)$  is different from zero only when the excited levels decay. Therefore this susceptibility is absent in nondissipative systems. This is in agreement with the phenomenological analysis of the electrooptic effect in chiral liquids and gases on the basis of the symmetry of the Onsager kinetic coefficients and the Kleinman rules.<sup>2,6</sup>

The mixed vector product of the dipole transition moments in Eq. (15) is different from zero only when all three vectors are noncollinear and noncoplanar. Therefore the rules for combining actual excited states making a nonzero contribution to the susceptibility  $\chi(\omega)$  are different from the selection rules for purely electric- and magnetic-dipole transitions in linear optical spectra. Hence it may be concluded that the circular electro-dichroism spectra will be different from both the ordinary linear absorption spectra and the linear circular dichroism spectra. The CED spectra should thereby yield additional spectroscopic information about the structure of the excited states and ultimately the structure and conformation of chiral molecules, which is especially important for molecular biology.<sup>1</sup>

Near a resonance of an optical frequency  $\omega$  with an isolated level in a chiral molecule (for example,  $\omega_{kg}$ :  $\omega = \omega_{kg} + \Delta_{kg}\Gamma_{kg}$ , where  $\Delta_{kg} \equiv (\omega - \omega_{kg})/\Gamma_{kg} < 1$ ) the electro-dichroism line is almost Lorentzian:

$$\operatorname{Re}\{\chi^{R_{kg}}(\Delta_{kg})\} \approx -\frac{1}{1+\Delta_{kg}^2} \frac{4}{3} NL^3 \left\{ \frac{\Gamma_{kg}}{\omega_{kg}} \Delta_{kg} \sum_{j \neq k} \frac{1}{\omega_{jg}^2 - \omega_{kg}^2} + \frac{1}{2\Gamma_{kg}} \sum_{j \neq k} \frac{\Gamma_{jg}}{\omega_{jg}^2} \right\} \\ \times (\mathbf{R}_{gk} \cdot [\mathbf{R}_{kj} \times \mathbf{R}_{jg}]) \quad (17)$$

(here the terms  $\sim K'$ ,  $K'^*$  from Eq. (15) have been neglected).

Of course, it is virtually impossible to estimate from Eqs. (15) and (17)  $\chi(\omega)$  for real molecules with a complicated spectrum. However, such an estimate can be obtained from the results of measurements of the preresonance susceptibility  $\chi^{(2)}(\omega; \omega_1, \omega_2)$  in saturated solutions of chiral arabinose<sup>15,18</sup> and  $\alpha$ -cyclodextrin<sup>5</sup> molecules and it can be assumed that  $\chi^{(2)}$  changes very little as  $\omega_2 \rightarrow 0$ . In this case, the equation (13) gives for the electrochromism coefficient  $\Delta\alpha \approx 0.02 \text{ cm}^{-1}$  for arabinose and  $0.08 \text{ cm}^{-1}$  for  $\alpha$ -cyclodextrin with  $E_0 = 30 \text{ kV/cm}$  and  $\lambda = 0.3 \text{ }\mu\text{m}$ ,  $n_0 \approx 1.5$ . These values of  $\Delta\alpha$  are adequate for reliable experimental detection of the effect.

5. In summary, this letter points to the existence of a new, as yet experimentally undetected, electrooptic effect in liquids and gases consisting of nonracemic mixtures of chiral molecules — circular electrochromism. In contrast to the standard circular dichroism, CED is linearly related with the intensity of the longitudinal electrostatic field and changes sign when the direction of the field is reversed. This makes it possible to use modulation spectroscopy and synchronous detection to detect this effect experimentally. The CED effect is also linear in the amplitude of the optical field and does not require the use of laser radiation. At the present time, experiments on the observation of this effect are being conducted in our laboratory.

I am grateful to A. Yu. Chikishev, N. N. Brandt, A. P. Shkurinov, V. A. Makarov, K. M. Drabovich, and T. M. Il'inoва for some stimulating discussions.

- <sup>1</sup>V. A. Avetisov and V. I. Gol'danskiĭ, *Usp. Fiz. Nauk* **166**, 873 (1996).  
<sup>2</sup>N. B. Baranov, Yu. V. Bogdanov, and B. Ya. Zel'dovich, *Usp. Fiz. Nauk* **123**, 349 (1977) [*Sov. Phys. Usp.* **20**, 870 (1977)].  
<sup>3</sup>N. I. Koroteev in *Frontiers in Nonlinear Optics, The Sergei Akhmanov Memorial Volume*, edited by H. Walther, N. Koroteev, and M. Scully, Inst. of Phys. Publishing, Bristol 1993, p. 228.  
<sup>4</sup>J. Giordmaine, *Phys. Rev. A* **138**, 1599 (1965).  
<sup>5</sup>A. V. Dubrovskii, N. I. Koroteev, and A. P. Shkurinov, *JETP Lett.* **56**, 551 (1992).  
<sup>6</sup>N. I. Koroteev, *Zh. Ėksp. Teor. Fiz.* **106**, 1260 (1994) [*JETP* **79**, 681 (1994)].  
<sup>7</sup>R. Zawodny, S. Woźniak, and G. Wagnière, *Opt. Commun.* **130**, 163 (1996).  
<sup>8</sup>J. D. Byers, H. I. Yee, and J. M. Hicks, *J. Chem. Phys.* **101**, 6233 (1994).  
<sup>9</sup>T. Verbiest, M. Kauranen, A. Persoons *et al.*, *J. Am. Chem. Soc.* **116**, 9203 (1994).  
<sup>10</sup>R. Stolle, M. Loddoch, and G. Marowsky, *Nonlinear Opt. – Princ. Mater. Phenom. Dev.* **8**, 79 (1994).  
<sup>11</sup>N. I. Koroteev, V. A. Makarov, and S. N. Volkov, *Nonlinear Opt. – Princ. Mater. Phenom. Dev.* **17**, 247 (1997).  
<sup>12</sup>A. V. Balakin, D. Bushe, N. I. Koroteev *et al.*, *JETP Lett.* **64**, 718 (1996).  
<sup>13</sup>S. Woźniak and G. Wagnière, *Opt. Commun.* **114**, 131 (1995).  
<sup>14</sup>N. Bloembergen, *Nonlinear Optics*, Benjamin, New York, 1965 [Russian translation, Mir, Moscow, 1966].  
<sup>15</sup>R. W. Boyd, *Nonlinear Optics*, Academic Press, San Diego, 1992.  
<sup>16</sup>Y. R. Shen, *The Principles of Nonlinear Optics*, Wiley, New York, 1984 [Russian translation, Mir, Moscow, 1989].  
<sup>17</sup>N. Bloembergen, H. Lotem, and R. T. Lynch, *Indian J. Pure Appl. Phys.* **16**, 151 (1978).  
<sup>18</sup>P. M. Rentzepis, J. A. Giordmaine, and K. W. Wecht, *Phys. Rev. Lett.* **16**, 792 (1966).

Translated by M. E. Alferieff

# Powerful thermonuclear neutron source based on laser excitation of hydrothermal dissipation in a volume-structured medium

S. Yu. Gus'kov and V. B. Rozanov

*P. N. Levedev Physical Institute, Russian Academy of Sciences, 117924 Moscow, Russia*

N. V. Zmitrenko

*Institute of Mathematical Modeling, Russian Academy of Sciences, 125047 Moscow, Russia*

(Submitted 30 July 1997; resubmitted 24 September 1997)

*Pis'ma Zh. Éksp. Teor. Fiz.* **66**, No. 8, 521–526 (25 October 1997)

An efficient method is proposed for generating thermonuclear neutrons by irradiating with a laser pulse a volume-structured material of subcritical density, consisting of a series of thin layers of condensed matter separated by interlayers of low-density matter (or a vacuum gap). The plasma ions are heated up to thermonuclear temperatures much higher than the electron temperature by hydrothermal dissipation of the energy of the laser radiation, as a wave of thermal explosions of the layers propagates along the laser beam axis, followed by collisions of plasma counterflows with conversion of the kinetic energy into thermal energy of ions. Different variants of the targets and experimental conditions are discussed in order to demonstrate the proposed method of neutron generation. © 1997 American Institute of Physics.

[S0021-3640(97)00320-4]

PACS numbers: 52.50.Jm, 52.55.Pi

1. The ions in a plasma irradiated with a laser pulse can be heated as a result of relaxational or dissipative processes in which energy is transferred from electrons, which absorb the laser radiation, to ions. In addition, if electron–ion relaxation results in heating of the ions up to the electron temperature, then hydrothermal dissipation, in which the thermal energy of the plasma is converted first into the energy of hydrodynamic motion of the matter and then into the thermal energy of ions, can result in the formation of a plasma with ion temperature much higher than the electron temperature,  $T_i \gg T_e$ .

In the present letter, we propose a method, based on laser excitation of hydrothermal dissipation in a volume-structured material, for producing long-lived nonequilibrium plasma, in which the ionic component is predominantly heated, as a source of powerful neutron radiation.<sup>1</sup> Such matter with a regular or stochastic structure consists of solid particles separated by a low-density matter or vacuum gaps. The average density of the medium must be equal to or less than the critical plasma density corresponding to plasma resonance for the laser radiation employed and the particles must be small enough to satisfy the condition of a thermal explosion when they are heated by the laser pulse. We shall term such a medium an “antireflective dissipative medium” (ARDM).

In the present letter, we examine a variant of an ARDM with a regular arrangement of layers of a solid material which have the same thickness, contain a thermonuclear fuel, and are equally spaced by vacuum gaps.

As a result of a thermal explosion, plasma energy is converted into the energy of directed motion of the ions. After the layer is unloaded to a critical density the laser radiation passing through the medium gives rise to a thermal explosion of the next layer. When the oppositely moving plasma fluxes from adjoining layers collide, the kinetic energy is converted into the thermal energy of the ions. The propagation depth of such a wave in the ARDM equals the inverse-bremsstrahlung radiation absorption length in the subcritical plasma formed.

As a result of the large difference of the ion and electron masses, the ion thermalization time  $\tau_{ii}$  due to ion–ion collisions is much shorter than the electron–ion energy relaxation time  $\tau_{ei(E)} = m_i \tau_{ei} / 2m_e$  (Ref. 2):  $\tau_{ii} / \tau_{ei(E)} \approx (2m_e^{1/3} T_i / m_i^{1/3} T_e z^{4/3})^{3/2}$  ( $z$  is the degree of ionization). For this reason, hydrothermal dissipation in an ARDM can result in the formation of a nonequilibrium plasma in which the ion temperature is up to 10 times higher than the electron temperature.<sup>3</sup>

A limiting variant of a layered dissipative medium is a system of two layers. Maximum ion temperatures in a laser plasma of 8–10 keV and a neutron yield of up to  $10^{13}$  have been recorded in experiments with a spherical analog of such a target — an “exploding shell.”<sup>4</sup> From the standpoint of producing a thermonuclear plasma as a powerful source of thermonuclear neutrons, multilayer ARDMs are preferable to bilayer targets for two reasons. First, for fixed laser pulse energy the degree of conversion of the energy absorbed in the target into thermal energy of plasma ions (the hydrothermal dissipation efficiency) increases with the number of layers in the medium. Indeed, the energy absorbed by one layer does not participate in the dissipation process, since approximately one-half of the masses of the first and last layers disperses into the space surrounding the target. Second, for fixed laser radiation intensity multilayer ARDMs make it possible to entrain into the hydrothermal dissipation process much larger masses of material at a high laser energy level than in the case of a bilayer target. In a bilayer target the maximum thickness  $m_d$  of the layers is fixed by the condition for thermal explosion — the velocity of the heat-conduction wave must be higher than the sound velocity throughout the entire heating time of the layer:

$$m_d \equiv (\Delta_0 \rho_0)_d \cong V_e^2 \tau_{ei} \rho_0 / V_s. \quad (1)$$

Here  $V_e$  and  $V_s$  are, respectively, the thermal velocity of the electrons and the sound velocity in the heated region of the layer;  $\Delta_0$  and  $\rho_0$  are the initial thickness and density of the layer;  $\tau_{ei}$  is the electron–ion collision time<sup>2</sup>

$$\tau_{ei} \approx 3.4 \times 10^{-15} T_e^{3/2} A / z^2 \rho, \quad (2)$$

where  $A$  is the atomic number of the ions. Here and below  $\rho$  is given in  $\text{g/cm}^3$  and  $T$  in keV. For radiation with intensity  $I$ , the temperature in the nondispersing heated region can be estimated as  $T_e = T_i \sim B^{-1} (I / \rho_0)^{2/3}$  ( $B \approx 10^{15} (z+1) / A (\gamma-1)$  ergs/g·keV is the specific heat and  $\gamma$  is the ratio of specific heats).

In a multilayer medium the thicknesses of the individual layers can be chosen so that each layer satisfies the condition for a thermal explosion. Then the ARDM mass  $m_p$

entrained into a hydrothermal dissipation process corresponds to the inverse-bremsstrahlung absorption length  $h$  for laser radiation in a plasma with  $\rho \leq \rho_{\text{cr}}$

$$h \approx c \tau_{ei} (\omega_L / \omega_p)^2, \quad m_p = \rho h, \quad (3)$$

where  $c$  is the speed of light;  $\omega_p = (4\pi n_e e^2 / m_e)^{1/2}$  is the plasma frequency;  $n_e$ ,  $e$ , and  $m_e$  are, respectively, the electron density, charge, and mass;  $\omega_L$  is the frequency of the laser radiation; and,  $\rho_{\text{cr}} \approx 1.63 \times 10^{-3} A / z \lambda^2$  g/cm<sup>3</sup> (here and below the radiation wavelength  $\lambda$  is given in  $\mu\text{m}$ ).

Comparing Eqs. (1) and (3) for the same laser radiation intensity, when the ratio of the plasma temperatures of these targets equals  $(\rho_0 / \rho_{\text{cr}})^{2/3}$ , we obtain for the ratio of the limiting masses of a multilayer antireflective target (for definiteness, with  $\rho = \rho_{\text{cr}}$ ) and a bilayer target

$$\frac{m_p}{m_d} \cong \frac{c}{V_s} \left( \frac{V_s}{V_e} \right)^2 \frac{\rho_0}{\rho_{\text{cr}}}.$$

In this letter, all calculations for a high-temperature plasma consisting of light elements were performed in the complete ionization approximation with  $A/z \approx 2$  and  $\gamma = 5/3$ . Then

$$m_p / m_d \cong 2.5 \times 10^2 \lambda^{8/3} \rho_0^{4/3} / (I \lambda^2)^{1/3}.$$

Here and below  $I$  is given in  $10^{14}$  W/cm<sup>2</sup> and  $I \lambda^2$  in  $10^{14}$  W ·  $\mu\text{m}^2/\text{cm}^2$ . For  $I \lambda^2 = 1 - 10$  and  $\lambda = 0.35 \mu\text{m}$ , which are interesting for producing a high-temperature plasma, the ratio  $m_p / m_k$  equals 3–10 for light substances with  $\rho_0 = 0.2 - 1$  g/cm<sup>3</sup>.

The hydrothermal dissipation effect is used to obtain a high ion temperature in one other type of laser target — a target with an inverted corona (ICT).<sup>5</sup> In a ICT the layer of matter containing thermonuclear fuel is deposited on the inner surface of a massive shell and irradiated with laser beams, which are introduced into the target through a system of openings. However, the possibilities of ICTs as a neutron source are limited by the complicated method of irradiating the target and energy losses due to heat conduction into the massive shell.

A method of accelerating plasma fluxes that is closest to the method employed in the present work is discussed in Refs. 4 and 5. However, it should be noted that the idea of producing a thermonuclear plasma under the conditions of colliding plasma flows goes back to Ref. 6, where it was suggested that electrodynamic methods be used to accelerate the flows. Such methods are now actively used in combination with different kinds of magnetic traps (see the review in Ref. 7) as well as in the magnetoplasma compressor problem.<sup>8</sup> Furthermore, it could be possible to use collisions of plasma flows from electric discharges in periodic systems of flat electrodes to obtain plasma with a controllable extent along the axis of the system.

At the modern level of development of the technique of pulsed acceleration of matter, the method of collisions of plasma flows can be used to produce a plasma with  $n \tau \sim (10^{11} - 10^{12}) \text{s/cm}^3$ , which corresponds to thermonuclear gain  $10^{-3} - 10^{-2}$ . The gas-dynamic method of acceleration with laser heating of matter gives a higher energy concentration in the plasma flow ( $10^{14} - 10^{15}$  W/cm<sup>2</sup>) but a shorter acceleration time ( $\sim 10^{-9} - 10^{-8}$  s) than the electrodynamic method ( $10^{11} - 10^{12}$  W/cm<sup>2</sup> and  $\sim 10^{-6} - 10^{-5}$  s, respectively). As a result, up to velocities of  $\sim 10^8$  cm/s, corresponding to an energy of

colliding nuclei  $\sim 20$  keV, the gas-dynamic method with laser heating can accelerate flows with a much higher particle density  $n \sim 10^{20} - 10^{21} \text{ cm}^{-3}$  but much lower particle interaction time  $\tau \sim 10^{-9}$  s than the electrodynamic method:  $n \sim 10^{17} - 10^{18} \text{ cm}^{-3}$  and  $\tau \sim 10^{-6}$  s.

2. We shall estimate the parameters of a nonequilibrium laser plasma of multilayer ARDMs for a medium whose average density equals the critical density. Such a material, having the maximum admissible density for ARDMs, gives a high hydrothermal dissipation efficiency.

We shall assume that laser radiation is absorbed in an individual layer before the moment of ‘‘antireflection,’’ when the density of the layer becomes equal to the critical density, after which the layer becomes transparent. According to the self-similar isothermal-dispersion solution,<sup>9</sup> the thermal energy  $E_h$  of the plasma is converted into the kinetic energy  $E_k$  of the ions with efficiency  $\beta_c \equiv E_k/E_h = 3(\gamma - 1)/(3\gamma - 1)$ . For  $\gamma = 5/3$  we have  $\beta_c = 1/2$ .

Assuming that the mass-average ion velocity for a layer is  $V_i = (2\beta_c I t / \rho_0 \Delta_0)^{1/2}$ , we easily obtain for the kinetic energy of an ion at the moment of ‘‘antireflection’’

$$\epsilon_k \approx \frac{m_i}{2} \left( \frac{3I\beta_c}{\rho_{cr}} \right)^{2/3}. \quad (4)$$

Hence follows for the average ion and electron temperatures in the plasma

$$T_i \equiv (\gamma - 1) \frac{\epsilon_k}{k} \cong 1.32A(I\lambda^2)^{2/3}, \quad T_e \equiv \frac{(1 - \beta_c)}{\beta_c} \frac{T_i}{z} \cong 2.64(I\lambda^2)^{2/3}, \quad (5)$$

where  $k$  is Boltzmann’s constant.

In the case of a collision of relatively dense laser ARDM plasma flows, the ions thermalize mainly by means of ion–ion collisions. Furthermore, collective processes associated with the development of a two-beam ion instability can make an additional contribution to the ion thermalization process. The ion relaxation time due to the inverse Landau damping on ion-acoustic waves can be estimated, on the basis of the linear theory,<sup>10</sup> as

$$\tau_{di} \approx 2(4\epsilon_k/T_b)^2 \omega_{pi}^{-1},$$

where  $\omega_{pi}$  is the ion plasma frequency and  $T_b$  is the temperature of the ions in the flow. Using the expression for the ion–ion relaxation time (see above), we have

$$\frac{\tau_{ii}}{\tau_{di}} \approx 1.5 \left( \frac{T_b}{\epsilon_k} \right)^2 \frac{\epsilon_k^{3/2}}{z^3 \rho^{1/2}} \left( \frac{A}{z} \right)^{1/2}.$$

For the conditions studied in the present letter, relevant to a laser pulse acting on an ARDM, viz.,  $\rho \approx 0.003 - 0.03 \text{ g/cm}^3$ ,  $\epsilon_k/T \approx 10 - 20$ , and  $\epsilon_k \approx 10 - 20$  keV, the contribution of the two-beam instability to the thermalization process equals 10–30%.

The conditions for matching the laser beam and ARDM parameters so as to obtain the maximum possible plasma mass and plasma confinement time are that the laser pulse duration  $\tau_L$  must equal the propagation time of thermal-explosion waves to the

bremsstrahlung absorption depth of the laser radiation  $\tau_L = t_h$  ( $t_h = h/V_i$ ) and that the diameter of the laser beam must be greater than the longitudinal extent of the plasma,  $2R_L \geq h$  (the condition that the energy losses due to lateral expansion of the plasma must be small). According to Eqs. (4) and (5), when these conditions are satisfied, the mass and lifetime of the plasma produced equal, respectively.

$$m_p \equiv \rho_{cr} h \approx 2 \times 10^{-3} I \lambda^2 / A \text{ g/cm}^2, \quad t_h = \tau_L \approx 9.4 \times 10^{-9} \lambda^2 (I \lambda^2)^{2/3} / A \text{ s.} \quad (6)$$

Hence the radius of a laser beam with duration  $\tau_L = t_h$  is

$$R_L \approx 5.4 \times 10^{-4} E_L^{1/2} A^{1/2} (I \lambda^2)^{-5/6} \text{ cm.} \quad (7)$$

Here and below, the laser pulse energy  $E_L$  is given in J. Using Eq. (7), we find that the matching conditions hold when

$$E_L \geq 2.95 \times 10^5 \lambda^4 (I \lambda^2)^{11/3} / A^3 \text{ J.} \quad (8)$$

We shall consider as the ARDM a target consisting of  $(\text{CD})_n$  layers ( $\rho_0 \approx 1 \text{ g/cm}^3$ ,  $A=7$ , deuterium concentration  $C_D=1/2$ ), BeDT layers ( $\rho_0 \approx 1 \text{ g/cm}^3$ ,  $A=14/3$ ,  $C_D=C_T=1/3$ ), and plastic  $(\text{CH})_n$  layers, onto both surfaces of which DT ice layers of equal thickness are frozen, with a mass content of 2/3 of the  $(\text{CH})_{1/3}(\text{DT})_{2/3}$  target ( $\rho_0 \approx 0.27 \text{ g/cm}^3$ ,  $A=3.1$ ,  $C_D=C_T=0.42$ ).

According to Eqs. (5) and (6), for example, for a  $(\text{CH})_{1/3}(\text{DT})_{2/3}$  target,  $T_i \approx 5 \text{ keV}$ ,  $T_e \approx 2.6 \text{ keV}$  with  $I \lambda^2 = 1$  and  $T_i \approx 23 \text{ keV}$ ,  $T_e \approx 14 \text{ keV}$  with  $I \lambda^2 = 10$  and the plasma mass and lifetimes are  $7 \times 10^{-4} \text{ g/cm}^2$  and 380 ps with  $I \lambda^2 = 1$  ( $\lambda = 0.35 \text{ } \mu\text{m}$ ,  $I \sim 10^{15} \text{ W/cm}^2$ ) and  $7 \times 10^{-3} \text{ g/cm}^2$  and 1.8 ns with  $I \lambda^2 = 10$  ( $\lambda = 0.35 \text{ } \mu\text{m}$ ,  $I \sim 10^{16} \text{ W/cm}^2$ ).

In the next section, we calculate the neutron yield in the approximation of a Maxwellian ion distribution in the ARDM plasma. However, it should be noted that a more accurate calculation should include the contribution of reactions of fast-ion groups that can form as a result of collective processes at the stages of interaction of the laser radiation with the matter for  $I \lambda^2 > 1$  and collision of the plasma flows.

**3. Approximating the temperature dependence of the DT and DD reaction rates as a power-law function with exponent 7/3 and  $T_i = 5 - 30 \text{ keV}$ , we obtain for the neutron yield with a matched laser pulse irradiating a multilayer ARDM**

$$N = 6.2 \times 10^{28} W_{12} C_1 C_2 E_L (I \lambda^2)^{14/9} A^{-2/3}.$$

Here  $C_i$  are the concentrations of the plasma nuclei participating in the fusion reaction,  $W_{\text{DT}} = 4 \times 10^{-19} \text{ cm}^3/\text{s}$ , and  $W_{\text{DD}} = 4 \times 10^{-21} \text{ cm}^3/\text{s}$ .

Plots of the neutron yield for targets consisting of  $(\text{CD})_n$  and  $(\text{CH})_{1/3}(\text{DT})_{2/3}$  layers versus the energy of the matched laser pulse are displayed in Fig. 1. For energies below the limiting values the neutron yield is lower than for a matched pulse as a result of energy losses due to the lateral dispersion of the plasma. Specifically, the data on Fig. 1 show that in the case of an ARDM the yield of DT neutrons  $10^{16}$  (with thermonuclear gain  $G \sim 0.1$ ) can be reached with laser radiation at the third harmonic of the ND laser  $\sim 400 \text{ kJ}$  and intensity  $5 \times 10^{15} \text{ W/cm}^2$  ( $I \lambda^2 = 5$ ). According to Eqs. (8) and (9) the pulse duration and beam radius should equal  $\sim 1.2 \text{ ns}$  and  $450 \text{ } \mu\text{m}$ , respectively. The computational results, obtained with the one-dimensional code Diana (described in Ref. 1), for targets consisting of ten alternating  $(\text{CD})_n$  and BeDT layers  $1 \text{ } \mu\text{m}$  thick, with different

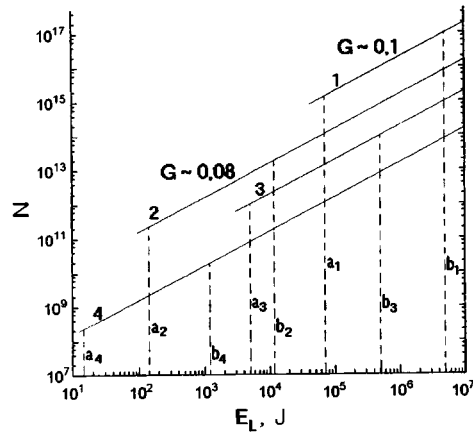


FIG. 1. Neutron yield versus energy of a matched laser beam for an ARDM consisting of  $(\text{CH})_{1/3}(\text{DT})_{2/3}$  layers (straight lines 1 ( $I\lambda^2=5$ ) and 2 ( $I\lambda^2=1$ )) and  $(\text{CD})_n$  layers (straight lines 3 ( $I\lambda^2=5$ ) and 4 ( $I\lambda^2=1$ )). The dashed straight lines  $a_i$  and  $b_i$  are the limiting energies, respectively, for wavelengths  $\lambda=0.35$  and  $1.06 \mu\text{m}$ .

spacing-to-thickness (aspect) ratios are presented in Fig. 2. The calculations were performed for the energy of the third harmonic of a Nd laser  $409 \text{ kJ/cm}^2$  and a pulse duration of  $300 \text{ ps}$  ( $I\lambda^2=1.5$ ). The computational results clearly demonstrate the hydrothermal dissipation effect ( $T_i/T_e \approx 2.5$  for a target consisting of BeDT layers and  $T_i/T_e \approx 4$  for a target consisting of  $(\text{CD})_n$  layers) and confirm the possibility of intense generation of thermonuclear neutrons in an ARDM laser plasma.

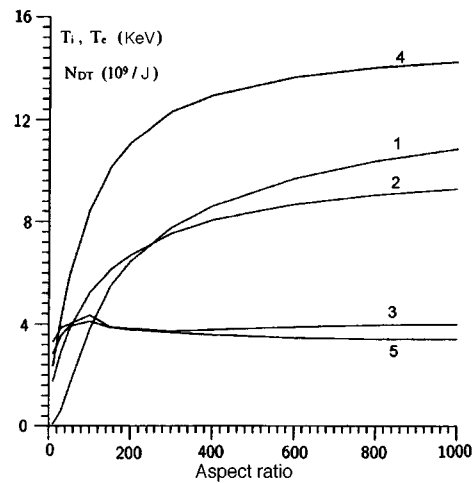


FIG. 2. Specific neutron yield per joule of laser energy for a BeDT target (1) and average ion temperature (curves 2 — BeDT target, 4 —  $(\text{CD})_n$  target) and electron temperature (curves 3 — BeDT target, 5 —  $(\text{CD})_n$  target) in the central cells of the targets as a function of the aspect ratio. The specific neutron yield for a  $(\text{CD})_n$  target is 120–150 times lower than for a BeDT target.

We note that a higher neutron yield with the gain increasing to 1–5 can be obtained by making the ARDM structure and the target construction more complicated. One variant of such a target could be a massive shell–container containing an opening for introducing the laser beam and filled with a shell ARDM (approximately 1  $\mu\text{m}$  thick and 100  $\mu\text{m}$  in diameter adjoining “exploding shells” consisting of a material containing thermonuclear fuel). Replacing a layered ARDM by a shell structure could increase the gain by a factor of 10–15 as a result of compression of the plasma during spherical cumulation of the shells and the presence of the container can increase the gain by another factor of 2–4 as a result of an increase in the plasma confinement time.

In summary, there is a possibility of producing a powerful source of thermonuclear neutrons in a simple one-beam target irradiation scheme by irradiating with a laser pulse targets containing antireflective dissipative media.

This work was supported by the International Science and Technology Center (Grant 029-94).

- <sup>1</sup>S. Yu. Gus'kov, V. B. Rozanov, and N. V. Zmitrenko, *Zh. Éksp. Teor. Fiz.* **108**, 548 (1995) [*JETP* **81**, 296 (1995)].
- <sup>2</sup>S. I. Braginskii, “Transport phenomena in plasmas,” in *Reviews of Plasma Physics*, edited by M. A. Leontovich, Vol. 1, Consultants Bureau, New York, 1963 [Russian original, Atomizdat, Moscow, 1963, p. 183].
- <sup>3</sup>S. Yu. Gus'kov, N. N. Demchenko, V. B. Rozanov *et al.*, *Abstracts of the 24th Conference on Plasma Physics and Controlled Thermonuclear Fusion, Zvenigorod, 1997* [in Russian], RIAS P. N. Lebedev Physics Institute, Russian Academy of Sciences, Moscow, 1997, p. 94.
- <sup>4</sup>E. K. Storm, *Laser Program Annual Report*, LLNL UCRL-50021-76, p. 83.
- <sup>5</sup>A. V. Bessarab, V. A. Gaïdash, G. V. Dolgoleva *et al.* *Zh. Éksp. Teor. Fiz.* **102**, 1800 (1992) [*Sov. Phys. JETP* **75**, 970 (1992)].
- <sup>6</sup>L. A. Artsimovich, S. Yu. Luk'yanov, I. M. Podgornyĭ, and S. A. Chuvatin, *Zh. Éksp. Teor. Fiz.* **33**, 3 (1957) [*Sov. Phys. JETP* **6**, 1 (1958)].
- <sup>7</sup>I. K. Konkashbaev, Yu. M. Skvortsov, and F. R. Ulinich, in *Progress in Science and Technology, Series on Plasma Physics* [in Russian], VINITI, Moscow, 1989, Vol. 9, p. 55.
- <sup>8</sup>A. I. Morozov, *Vest. Akad. Nauk SSSR* **6**, 28 (1969).
- <sup>9</sup>V. S. Imshennik, *Dokl. Akad. Nauk SSSR* **131**, 1287 (1959) [*Sov. Phys. Dokl.* **5**, 253 (1960)].
- <sup>10</sup>E. M. Lifshitz and L. P. Pitaevskii, *Physical Kinetics*, Pergamon Press, New York, 1981 [Russian original, Nauka, Moscow, 1979, p. 248].

Translated by M. E. Alferieff

# Manifestations of the Larkin–Ovchinnikov–Fulde–Ferrell state in bimetal ferromagnet–superconductor structures

Yu. N. Proshin and M. G. Khusainov<sup>a)</sup>

*Kazan State University, 420008 Kazan, Russia*

(Submitted 26 August 1997)

*Pis'ma Zh. Éksp. Teor. Fiz.* **66**, No. 8, 527–532 (25 October 1997)

Reentrant and periodically reentrant superconductivity in contacts and ferromagnet/superconductor (F/S) superlattices are predicted on the basis of the theory developed in this letter. These effects are consequences of the realization of the Larkin–Ovchinnikov–Fulde–Ferrell state in F layers. An explanation is given for the qualitatively different behavior of the critical temperature observed by different experimental groups on identical F/S structures. © 1997 American Institute of Physics. [S0021-3640(97)00420-9]

PACS numbers: 74.20.–z, 74.80.Dm, 75.50.Cc

Analysis of the latest experiments<sup>1–5</sup> with ferromagnet/superconductor (F/S) multilayers shows a qualitatively different behavior of the critical temperature  $T_c$  as a function of the thickness  $d_f$  of the ferromagnetic interlayers in the same F/S structures. Specifically, in some experiments on the systems Fe/V (Ref. 1) and Gd/Nb (Ref. 2) after decreasing rapidly at the outset,  $T_c$  reaches a plateau as  $d_f$  increases, whereas in other experiments on the same systems (Refs. 3 and Refs. 4 and 5, respectively) the plateau is preceded by an oscillatory behavior of  $T_c(d_f)$ . The theoretical interpretation given in Refs. 6 and 7 for the oscillations in  $T_c(d_f)$  reduce to a periodic “switching” of the type of superconductivity from the traditional 0 phase to a  $\pi$  phase, where the sign of the order parameter  $\Delta$  changes on passage through the F interlayer. However, the limitations of Refs. 6 and 7 make it impossible to give a unified description of the two different types of behavior of  $T_c(d_f)$ . Furthermore, it was recently discovered that oscillations of  $T_c(d_f)$  also occur in the trilayer structure Fe/Nb/Fe,<sup>8</sup> where  $\pi$ -phase superconductivity is impossible. This requires a new formulation of the question of the nature of the nonmonotonic dependence of  $T_c(d_f)$  in F/S systems and a theory that adequately describes the existing experimental data.

The strong exchange field in ferromagnetic layers makes it necessary to take account of two important points. First, an important condition for conservation of superconductivity in F/S systems, together with a large thickness  $d_s$  of the S layers ( $d_s \gg d_f$ ), is that the transmittance of the F/S boundaries must be moderate, not too high. However, the boundary conditions for the pair amplitude with arbitrary transmittance of the F/S boundary are still unknown.<sup>6</sup> Second, as a result of the proximity effect, pair correlations are also induced in F layers, but the large exchange splitting  $2I \gg \pi T_c$  of the Fermi level changes the pairing condition. According to Larkin–Ovchinnikov–Fulde–Ferrell

(LOFF),<sup>9,10</sup> quasiparticles from energy states  $\mathbf{p}, \uparrow$  and  $-\mathbf{p}+\mathbf{k}, \downarrow$  with momenta of different absolute magnitude, where  $k \approx 2I/v_f$  and  $v_f$  is the Fermi velocity, will be paired in the ferromagnet. Nonmagnetic-impurity scattering with the rate  $\tau_f^{-1}$ , which has no effect on BCS pairing with zero total momentum, will impede the appearance of the LOFF phase in F layers. For this reason, the pair amplitude in ferromagnetic layers should oscillate with period  $a_f = k^{-1}$ , decaying over the mean free path length  $l_f = v_f \tau_f$  from the F/S boundary.

It will be shown below that oscillations of the pair amplitude will lead to a periodic compensation of the paramagnetic effect of the exchange field, giving rise to oscillations in  $T_c(d_f)$  not only in multilayer but also in bilayer F/S contacts. The observability of these oscillations, a striking manifestation of which could be periodically reentrant superconductivity, strongly depends on the purity of the F layers and the transmittance of the F/S boundaries.

Let us consider first a planar contact between a ferromagnetic metal occupying the region  $-d_f < z < 0$  and a superconductor occupying the region  $0 < z < d_s$ . Near a second-order phase transition point,  $T_c$  of the F/S contact is determined from the Gor'kov integral equation for the order parameter  $\Delta(z)$  of a nonuniform system, written for convenience in terms of the anomalous Usadel function  $F_{\alpha\beta}(z, \omega)$ :

$$\Delta(z) = \lambda(z) \pi T \operatorname{Re} \sum_{\omega}^{\prime} F_{\alpha\beta}(z, \omega), \quad (1)$$

$$F_{\alpha\beta}(z, \omega) = \frac{1}{\pi N(z)} \int_{-d_f}^{d_s} H_{\alpha\beta}(z, z', \omega) \Delta(z') dz', \quad (2)$$

where  $\lambda(z > 0) = \lambda_s$  and  $\lambda(z < 0) = \lambda_f$  are dimensionless parameters of the electron-electronic interaction;  $N(z)$  is the density of states at the Fermi level;  $\alpha$  and  $\beta$  are spin indices ( $\alpha \neq \beta$ ); a prime on the sum indicates a cutoff at the Debye frequency  $\omega_D$ ;  $T$  is the temperature; and,  $\omega = \pi T(2n + 1)$  is the Matsubara frequency. It can be shown by diagrammatic methods<sup>11</sup> that in the presence of an exchange field and nonmagnetic-impurity scattering the correlation function  $H_{\alpha\beta}(z, z', \omega)$  is the solution of another integral equation

$$H_{\alpha\beta}(z, z', \omega) = K_{\alpha\beta}(z, z', \omega) + \int_{-d_f}^{d_s} \frac{K_{\alpha\beta}(z, z_1, \omega) H_{\alpha\beta}(z_1, z', \omega)}{2\pi N(z_1) \tau(z_1)} dz_1 \quad (3)$$

(cf. Ref. 12). Here we have introduced the notation

$$K_{\alpha\beta}(z, z', \omega) = \int \frac{d^2 p}{(2\pi)^2} G_{\alpha\alpha}(\mathbf{p}, z, z', \omega) G_{\beta\beta}(\mathbf{p}, z, z', -\omega), \quad (4)$$

$G_{\alpha\alpha}(\mathbf{p}, z, z', \omega)$  is the Green's function of the conduction electrons in the normal phase,  $\mathbf{p}$  is the two-dimensional momentum in the contact plane, and  $\tau^{-1}(z)$  is the impurity scattering rate, which, like  $N(z)$ , changes abruptly at a transition through the interface  $z = 0$  of the metals. Next, by solving for  $K_{\alpha\beta}(z, z', \omega)$ , in the spirit of Ref. 12, the problem with a potential barrier at the F/S interface as well, it can be shown that in the

“dirty” limit the system of integral equations (2) and (3) reduces to a boundary-value problem for the function  $F_{\alpha\beta}(z, \omega)$ . The latter problem includes the differential equation

$$\left[ |\omega| + iI(z)g_{\alpha\beta} \sin n\omega - \frac{1}{2}D_{\alpha\beta}(z) \frac{\partial^2}{\partial z^2} \right] F_{\alpha\beta}(z, \omega) = \Delta(z) \quad (5)$$

with boundary conditions relating the flux of the function  $F_{\alpha\beta}(z, \omega)$  with its jump at the flat interface  $z=0$  of the metals

$$D_{j\alpha\beta} \frac{\partial F_{\alpha\beta}(z, \omega)}{\partial z} \Big|_{z=\pm 0} = \frac{\sigma_j v_j}{4} [F_{\alpha\beta}(+0, \omega) - F_{\alpha\beta}(-0, \omega)], \quad j=f, s. \quad (6)$$

Here  $\sigma_s$  and  $\sigma_f$  are the transmittances of the contact on the S and F metal sides and are related by the detailed balance relation  $\sigma_s v_s N_s = \sigma_f v_f N_f$  (Ref. 13),  $g_{\uparrow\downarrow} = -g_{\downarrow\uparrow} = 1$ , and the effective diffusion coefficient is given by the expression

$$D_{\alpha\beta}(z) = D(z) / [1 + 2i\tau(z)I(z)g_{\alpha\beta} \text{sign } \omega]; \quad D(z) = D_j = v_j l_j / 3, \quad (7)$$

where  $I(z < 0) = 1$  and  $I(z > 0) = 0$ . The equations (5) and (6) are valid for  $l_j < \zeta_j$ , where  $\zeta_j = \text{Re} \sqrt{D_j / 2\pi T + 2iI_j}$  is the coherence length of the  $j$ th metal.

The boundary-value problem (1), (5), (6) obtained for the proximity effect in a F/S contact differs from the previous problems<sup>6,7</sup> in two respects. First, the boundary conditions  $F(+0, \omega) = F(-0, \omega)$  employed in Refs. 6 and 7 are a particular case of Eq. (6) and correspond to the high-transmittance limit  $\sigma_j \gg l_j / \zeta_j$  i.e., the flux of  $F(z, \omega)$  through the F/S boundary is neglected. However,  $\sigma_j$  will depend strongly on the conditions and method of preparation of the F/S interface. It should either serve as an adjustable parameter of the theory or be measured experimentally. Second, the quasiparticle motion in the ferromagnet is of mixed diffusion–spin-wave character and is described by an effective complex-valued diffusion coefficient  $D_f^* = D_f / (1 + 2iI\tau_f)$  (Ref. 14), in contrast to Refs. 6 and 7.

The strong depairing effect of the exchange field  $I$  ( $I \gg \pi T_{cs}$ , where  $T_{cs}$  is the critical temperature of an isolated S layer) is the main mechanism leading to the destruction of superconductivity in F/S systems. Neglecting, as a simplification, the interaction in the F layer  $\lambda_f \approx 0$  ( $\Delta(z < 0) \approx 0$ ), we seek the solution of equations (1), (5), (6) in a form that excludes an electron flux through the outer boundaries of the contact, i.e.,  $F_s(z, \omega) \propto \cos k_s(z - d_s)$  for  $z > 0$  and  $F_f(z, \omega) \propto \cos k_f(z + d_f)$  for  $z < 0$ , where  $k_s$  and  $k_f$  do not depend on  $\omega$ . Then, we obtain the following closed system of equations for the reduced superconducting transition temperature  $t = T_c / T_{cs}$  of the F/S contact:

$$\ln t = \Psi\left(\frac{1}{2}\right) - \text{Re} \Psi\left(\frac{1}{2} + \frac{D_s k_s^2}{4\pi T_{cs} t}\right); \quad k_f^2 = \frac{-2iI}{D_f^*} = \frac{-2iI(1 + 2iI\tau_f)}{D_f}; \quad (8)$$

$$D_s k_s \tan k_s d_s = \frac{\sigma_s v_s}{4 - (\sigma_f v_f / D_f^* k_f) \cot k_f d_f},$$

where  $\Psi(x)$  is the digamma function. As follows from Eqs. (8), the depairing parameter  $D_s k_s^2$  and the critical temperature  $T_c$  depend strongly on the thickness of the layers, the

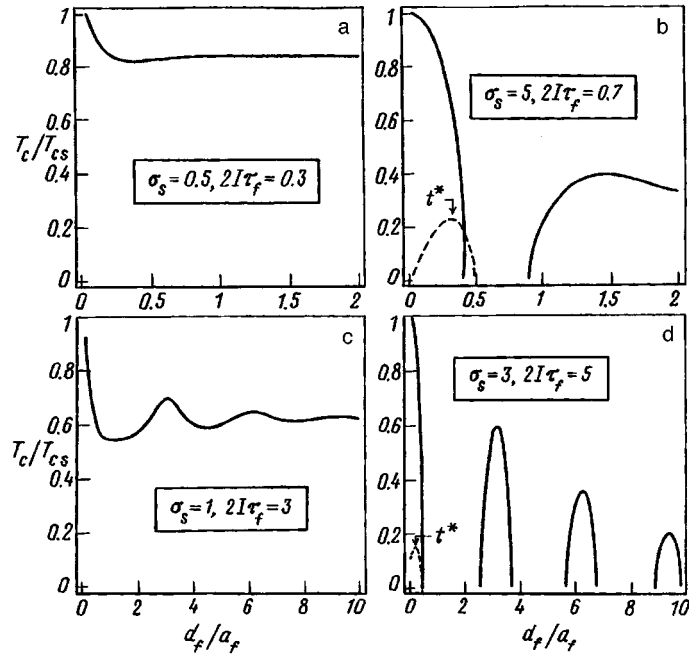


FIG. 1. Reduced superconducting transition temperature  $T_c/T_{cs}$  of a F/S contact versus the reduced thickness  $d_f/a_f$  of the ferromagnetic layer, as described by Eqs. (8) and (10) with  $N_s v_s = N_f v_f$ ,  $d_s = 500 \text{ \AA}$ , and  $\zeta_{s0} = 400 \text{ \AA}$ , where  $\zeta_{s0}$  is the BCS coherence length. The values of the parameters  $\sigma_s$  and  $2I\tau_f$  are presented on the same plots: a) emergence of  $T_c$  onto a plateau; b) reentrant superconductivity; c) oscillations of  $T_c$ ; d) periodically reentrant superconductivity. The dashed curves  $t^*$  in parts b and d represent lines of tricritical points.

transmittance of the F/S boundary, and the ratio between the exchange splitting  $2I$  of the Fermi level and the collision rate  $\tau_f^{-1}$  of electrons with nonmagnetic impurities in the ferromagnet.

The spatial variations of the Usadel function in the F layer are characterized by the wave number  $k_f = 1/\zeta_f' - i/\zeta_f''$ , where  $\zeta_f'$  is responsible for the period of the oscillations and  $\zeta_f''$  for the penetration depth of the pair amplitude in the ferromagnet. As one can see from Eq. (8), in the dirty limit  $l_f \ll a_f = v_f/2I$  these two lengths are approximately equal and differ only by small corrections of the order of  $I\tau_f$

$$\zeta_f' = \sqrt{D_f/I(1 - I\tau_f)}; \quad \zeta_f'' = \sqrt{D_f/I(1 + I\tau_f)}; \quad 2I\tau_f \ll 1. \quad (9)$$

A numerical analysis of the function  $T_c(d_f)$  for dirty F/S contacts with different values of the parameters  $\sigma_s$  and  $2I\tau_f$  is presented in Fig. 1a and b. As shown in Fig. 1a, in the case of weak transmittance and strong damping, the oscillations of the function  $F_f(z, \omega)$  are not observed and  $T_c$  continuously approaches a constant as  $d_f$  increases. Such a behavior of  $T_c(d_f)$  has been observed in Gd/Nb bilayers.<sup>2</sup> As  $\sigma_s$  and  $2I\tau_f$  increase, the function  $T_c(d_f)$  acquires a deep minimum, whose development can lead to reentrant superconductivity, depicted in Fig. 1b.

If  $2I\tau_f > 1$ , then the diffusion description which we employed above to describe quasiparticle motion in a ferromagnet is inapplicable,<sup>14</sup> though the standard condition for the dirty limit  $\pi T\tau_f \ll 1$  is satisfied. In this case, solving Eqs. (2)–(4) simultaneously shows that the asymptotic behavior of the function  $F_f(z, \omega)$  is described by a wave number  $k_f$  different from (8)

$$k_f^2 \approx \frac{-2iI(1+2iI\tau_f)}{v_f l_f}; \quad \zeta_f' \approx a_f = \frac{v_f}{2I}; \quad \zeta_f'' \approx 2l_f; \quad 2I\tau_f \gg 1, \quad (10)$$

where  $\text{Re } k_f$  is of the order of the pair momentum  $k$  in the LOFF state<sup>9,10</sup> and  $\text{Im } k_f \sim l_f^{-1}$  is the variance in the values of  $k$ , i.e., the damping. To describe the function  $T_c(d_f)$  in F/S contacts with relatively pure F layers ( $2I\tau_f > 1$ ),  $D_f$  in Eqs. (8) must be replaced by  $3D_f$ . The depairing factor  $D_s k_s^2$  and the critical temperature will oscillate with increasing  $d_f$  with a period determined by the spin stiffness  $a_f = k^{-1}$ . These oscillations will decay for  $d_f > 2l_f$  ( $\gg a_f$ ), driving  $T_c$  to a constant, as shown in Fig. 1c. This behavior of  $T_c(d_f)$  has been observed in Fe/Nb/Fe trilayers,<sup>8</sup> to which case the equations (8) can be extended by making the substitution  $d_s \Rightarrow d_s/2$ . It is interesting to note that for sufficiently large values of the parameters  $\sigma_s$  and  $2I\tau_f$  the superconductivity of the F/S contact will be periodically reentrant, as shown in Fig. 1d.

Superconductivity in a F/S contact is a combination of BCS pairing in the S layer and LOFF pairing<sup>9,10</sup> in the F layer. For a sign-constant pair amplitude  $F_s(z)$  in the S layer, the oscillations of the wing  $F_f(z)$  in the F layer against the background of a constant exchange field  $I$  are equivalent to a sinusoidal modulation of the latter. For this reason, the maxima in  $T_c(d_f)$  always appear when an even number of quarter waves  $\cos k_f(z+d_f)$  fit within the thickness of the F layer. When this number is odd, the paramagnetic effect of the uncompensated fourth suppresses the BCS pairing in the S layer, resulting in a minimum of  $T_c$  or destruction of superconductivity. This is expressed mathematically as a unique periodic modulation of the transmittance  $\sigma_s$  of the S/F boundary and the depairing parameter  $D_s k_s^2$  by the resonance denominator, containing  $\cot(k_f d_f)$ , in Eqs. (8). The presence of nonmagnetic scattering results in incomplete compensation of the exchange field incomplete and damped modulation of  $\sigma_s$  and  $T_c$  with increasing  $d_f$ .

In contrast to F/S contacts, the unit cell of a F/S superlattice can exist in two stable LOFF states differing by the parity of the pair amplitude relative to the center of the F layer: the 0 phase, with  $F_f(z, \omega) \propto \cos k_f(z+d_f/2)$ , and the  $\pi$  phase, with  $F_f(z, \omega) \propto \sin k_f(z+d_f/2)$ . The equations for  $T_c$  in the 0-phase case are obtained from Eqs. (8) by replacing  $d_j$  by  $d_j/2$ . To find  $T_c$  in the  $\pi$  case it is necessary, in addition, to replace the function  $\cot x$  on the right-hand side of the last of the equations (8) by  $-\tan x$ . The separation of the maxima of  $T_c$  by  $\pi \zeta_f'$  in the 0 and  $\pi$  states results in a competition between these states and alternation in the phase diagrams  $T_c(d_f)$ , see Fig. 2.

For  $\sigma_s \sim 2I\tau_f \sim 0.5$ , as one can see from Fig. 2a, a transition from the 0- to the  $\pi$ -phase branch of  $T_c(d_f)$  results in a single bump in  $T_c$ , just as in Gd/Nb multilayers.<sup>4,5</sup> For lower values of these quantities ( $\sigma_s \sim 2I\tau_f \sim 0.3$ ) the 0- and  $\pi$ -phase solutions in the region of “switching” approach one another and in Ref. 2, instead of a bump,  $T_c$  in the same Gd/Nb multilayers emerges onto a plateau. The difference between the results obtained in Refs. 2 and Refs. 4 and 5 is apparently due to the difference in the transmit-

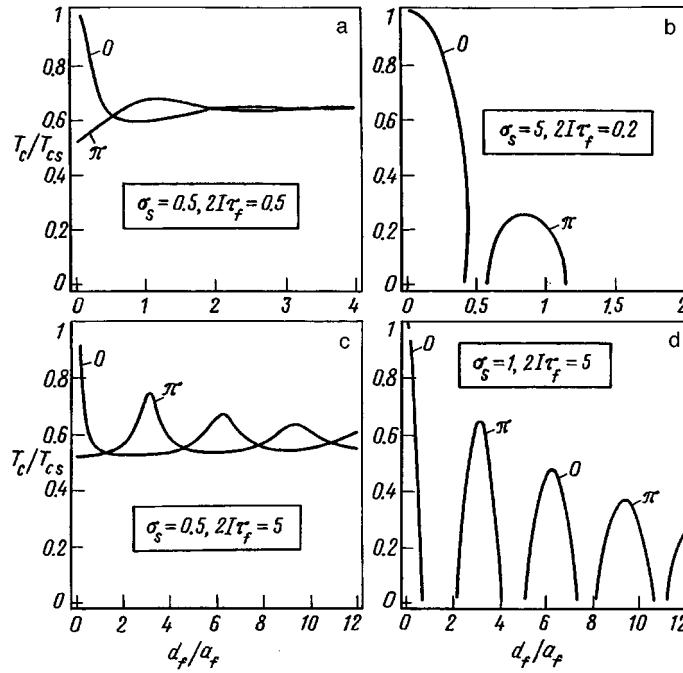


FIG. 2.  $T_c/T_{cs}(d_f/a_f)$  phase diagrams of a F/S superlattice with  $N_s v_s = N_f v_f$ , and  $d = 500 \text{ \AA}$ ;  $\xi_{s0}$  is the BCS coherence length. The values of the parameters  $\sigma_s$  and  $2I\tau_f$  are presented on the plots: a) single bump in  $T_c$ ; b) reentrant superconductivity; c) oscillations of  $T_c$  in the presence of competition between the 0- and  $\pi$ -phase states; d) periodically reentrant superconductivity with alternation of the 0- and  $\pi$ -phase peaks. The symbols 0 and  $\pi$  on the curves correspond to the 0- and  $\pi$ -phase states.

tance of the F/S boundaries and the purity of the F layers in the experimental Gd/Nd samples. The reentrant superconductivity arising with a high transmittance  $\sigma_s$ , as shown in Fig. 2b, is characterized by the fact that the  $d_f$ -limited 0 and  $\pi$  states adjoin one another.

For  $2I\tau_f > 1$  the oscillations of  $T_c(d_f)$  will be stronger, and their period in the 0- or  $\pi$ -phase cases, separately, will be two times larger than in the corresponding F/S contact. The effect of the competition between the 0- and  $\pi$ -phase states, which is shown in Figs. 2c and 2d, will be that the periods of the  $T_c$  oscillations will be formally identical in the superlattices and contacts. It would be interesting to check this experimentally, together with the other above-described manifestations of the LOFF states in F/S systems.

<sup>a)</sup>e-mail: mansur.khusainov@ksu.ru

<sup>1</sup>P. Koorewaar, Y. Suzuki, R. Coehoorn *et al.*, Phys. Rev. B **49** 441 (1994).

<sup>2</sup>C. Strunk, C. Surgers, U. Paschen *et al.*, Phys. Rev. B **49**, 4053 (1994).

<sup>3</sup>H. K. Wong, B. Y. Jin, H. Q. Yang *et al.*, J. Low Temp. Phys. **63**, 307 (1986).

<sup>4</sup>J. S. Jiang, D. Davidovic, D. H. Reich *et al.*, Phys. Rev. Lett. **74**, 314 (1995).

<sup>5</sup>J. S. Jiang, D. Davidovic, D. H. Reich *et al.*, Phys. Rev. B **54** 6119 (1996).

- <sup>6</sup>Z. Radovic, M. Ledvij, L. Dobrosavljevic-Grujic *et al.*, Phys. Rev. B **44**, 759 (1991).
- <sup>7</sup>A. I. Buzdin, B. Vučichich, and M. Yu. Kupriyanov, Zh. Éksp. Teor. Fiz. **101**, 231 (1992) [Sov. Phys. JETP **74**, 124 (1992)].
- <sup>8</sup>Th. Muhge, N. N. Garif'yanov, Yu. V. Goryunov *et al.*, Phys. Rev. Lett. **77**, 1857 (1996).
- <sup>9</sup>A. I. Larkin and Yu. N. Ovchinnikov, Zh. Éksp. Teor. Fiz. **47**, 1136 (1964) [Sov. Phys. JETP **20**, 762 (1965)].
- <sup>10</sup>P. Fulde and R. A. Ferrell, Phys. Rev. A **135**, 550 (1964).
- <sup>11</sup>A. A. Abrikosov, L. P. Gor'kov, and I. E. Dzyaloshinskiĭ, *Methods of Quantum Field Theory in Statistical Physics*, Prentice-Hall, Englewood Cliffs, N.J., 1963 [Russian original, Nauka, Moscow, 1962].
- <sup>12</sup>R. O. Zaitsev, Zh. Éksp. Teor. Fiz. **50**, 1055 (1966) [Sov. Phys. JETP **23**, 702 (1966)].
- <sup>13</sup>M. G. Khusainov, JETP Lett. **53**, 579 (1991).
- <sup>14</sup>P. Fulde and A. Luther, Phys. Rev. **175**, 337 (1968).

Translated by M. E. Alferieff

# Theory of the pseudogap in the elementary excitation spectrum of the normal phase of bilayer cuprates

S. V. Varlamov, M. V. Eremin, and I. M. Eremin

*Kazan State University, 420008 Kazan, Russia*

(Submitted 18 July 1997)

*Pis'ma Zh. Éksp. Teor. Fiz.* **66**, No. 8, 533–538 (25 October 1997)

Solutions of the integral equations for the pseudogap in the elementary excitation spectrum of current carriers in bilayer cuprates are found. In the general case, the pseudogap possesses  $s + id$  symmetry, where the  $s$  component is determined by the interaction of holes via the phonon field and the  $d$  component is due to the superexchange interaction of the copper spins and the Coulomb-repulsion screened holes. The  $s$  and  $d$  components exhibit different temperature dependences. This fact enabled us to explain the characteristic features of the temperature behavior of the normal-phase spin susceptibility of lightly doped cuprates, specifically, for the compound  $\text{YBa}_2\text{Cu}_4\text{O}_8$  in the entire temperature interval  $T > T_c$ . The wave-number dependence of the pseudogap agrees with the photoemission data for  $\text{Bi}_2\text{Sr}_2\text{CaCu}_2\text{O}_{8+y}$ . © 1997 American Institute of Physics. [S0021-3640(97)00520-3]

PACS numbers: 74.25.Jb, 74.25.Gz, 74.72.Bk

The problem of the electronic structure of superconductors based on  $\text{CuO}_2$  planes is the focus of modern investigations. Recent photoemission experiments<sup>1,2</sup> have revealed especially clearly the presence of a pseudogap in the elementary excitation spectrum of the normal phase of  $\text{Bi}_2\text{Sr}_2\text{CaCu}_2\text{O}_{8+y}$  with low doping indices. The presence of a pseudogap in the normal phase of underdoped cuprates qualitatively explains the anomalies of many physical properties of high- $T_c$  superconductors,<sup>3,4</sup> but the origin of the pseudogap remains unknown. It has been suggested in a number of works that the pseudogap is due to instability of the quasi-Fermi-liquid subsystem with respect to charge- or spin-density waves.<sup>5</sup> In Ref. 6 the pseudogap is attributed to spin pairing and in Ref. 7 it is attributed to strong phase fluctuations of the standard order parameter (of Cooper pairs), which in the opinion of the authors appear long before the superconducting transition temperature.

The reasons for the instability — interaction via the phonon field, superexchange interaction of copper spins, and Coulomb repulsion of holes — are ordinarily analyzed separately because of the difficulty of the problem. At the same time, the integral equations for the pseudogap are nonlinear and therefore the result of performing a simultaneous analysis of these interactions is not obvious.

This letter reports the first results of solving the system of nonlinear integral equations for the pseudogap taking all three interactions into account at the same time. It was found that unlike  $s$ -type solutions for the order parameter of charge-density waves asso-

ciated with the phonon mechanism<sup>8</sup> and  $d$ -type solutions associated with superexchange,<sup>9</sup> in the general case the solutions are complex-valued and possess  $s + id$  symmetry. Furthermore, as will be shown below, the real ( $s$ ) and imaginary ( $d$ ) components have different temperature dependences. The critical temperature  $T_{ex}^*$  for the  $d$  component can be several times higher than  $T_{ph}^*$  for the  $s$  component, which enables us ultimately to describe the temperature dependence of the spin susceptibility of bilayer cuprates, specifically, for  $\text{YBa}_2\text{Cu}_2\text{O}_8$ , from  $T_c = 82$  K up to  $T \approx 700$  K. The latter, as is well known, is most accurately measured by the NMR method via the Knight shift on the Cu(2) copper nuclei.

In Ref. 10 it was found that the photoemission data on the elementary excitation spectrum of the bilayer cuprates  $\text{YBa}_2\text{Cu}_4\text{O}_8$  and  $\text{YBa}_2\text{Cu}_3\text{O}_7$  (Ref. 11) can be completely described on the basis of the model of singlet-correlated motion of oxygen holes. The wave-number dependence of the quasiparticle energy can also be represented quite accurately in a two-band model,<sup>12,13</sup> equivalent to Ref. 10, in the following form:

$$\epsilon_k = 1/2 (E_k^{dd} + E_k^{pp}) + 1/2 [(E_k^{dd} - E_k^{pp})^2 + 4E_k^{pd}E_k^{dp}]^{1/2}, \quad (1)$$

where

$$E_k^{pp} = \epsilon_p - t_{ab} + \sum_m \left\{ \left[ P_p + \frac{1}{P_p} \langle S_i S_m \rangle \right] t_{im}^{(p)} - \frac{K_{im} + J_{im}/2}{P_p} \langle \Psi_i^{pd, \uparrow} \Psi_m^{\uparrow, pd} \rangle \right\} \exp(ikR_{im}), \quad (2)$$

$$E_k^{pd} = \sum_m \left[ P_d - \frac{1}{P_p} \langle S_i S_m \rangle \right] t_{im}^{(pd)} \exp(ikR_{im}), \quad (3)$$

and the expressions for  $E_k^{dd}$  and  $E_k^{dp}$  are obtained from the expressions presented for  $E_k^{pp}$  and  $E_k^{pd}$  by replacing the  $p$  indices by  $d$  and the correlation function  $\langle \Psi_i^{pd, \uparrow} \Psi_m^{\uparrow, pd} \rangle$  by  $\langle \Psi_i^{\downarrow, 0} \Psi_m^{0, \downarrow} \rangle$ . Just as in Refs. 12 and 13, the Hubbard-type operators  $\Psi_i^{pd, \uparrow}$  ( $\Psi_i^{\uparrow, pd}$ ) and  $\Psi_i^{\downarrow, 0}$  ( $\Psi_i^{0, \downarrow}$ ) correspond to the quasiparticle creation (annihilation) in singlet and copper bands, respectively. The average values of the anticommutators equal  $P_p = (2 + \delta)/4$  and  $P_d = (2 - \delta)/4$ , where  $\delta$  is the number of conduction holes per unit cell in the  $\text{Cu}_2\text{O}_4$  bilayer.  $K_{im}$  and  $J_{im}$  are the Coulomb and superexchange interaction parameters determined by expressions of the type

$$H_{Co} = \sum_{i>j} K_{ij} (1 - \Psi_i^{pd, pd} - \Psi_i^{0, 0}) (1 - \Psi_j^{pd, pd} - \Psi_j^{0, 0}), \quad (4)$$

$$H_{Ex} = \sum_{i>j} J_{ij} \left[ (S_i S_j) - \frac{n_i n_j}{4} \right], \quad (5)$$

where  $n_i = \Psi_i^{\uparrow, \uparrow} + \Psi_i^{\downarrow, \downarrow}$  is the number of spins per site in the copper sublattice.

Expression (1)–(3) describe the dispersion of the singlet bonding (odd) band. In the case of an antibonding (even) band, the tunneling parameter  $-t_{ab}$  in Eq. (2) is replaced by  $+t_{ab}$ .

The relative values of the transfer integrals (in meV), estimated in Ref. 12, between the first, second, and third neighbors equal:  $t_1^{(p)} = 82$ ,  $t_2^{(p)} = 3$ ,  $t_3^{(p)} = 12$ ,  $t_1^{(d)} = 79$ ,  $t_2^{(d)} = 7$ ,  $t_3^{(d)} = 10$ ,  $t_1^{(pd)} = 83$ ,  $t_2^{(pd)} = 6$ , and  $t_3^{(pd)} = 12$ . The dielectric gap and the spin correlation functions are taken as  $\epsilon_p - \epsilon_d = 1.4$  eV,  $\langle S_i S_j \rangle_1 = -0.14$ ,  $\langle S_i S_j \rangle_2 = 0.07$ , and

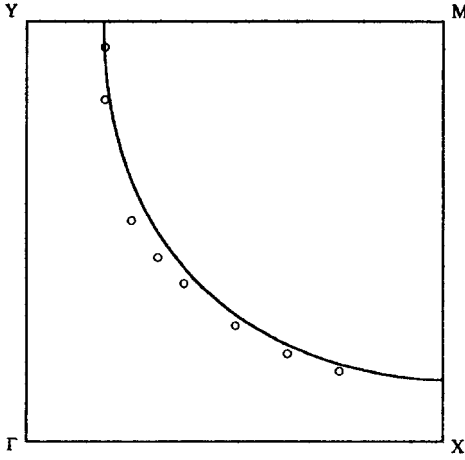


FIG. 1. Form of the Fermi surface of  $\text{Bi}_2\text{Sr}_2\text{CaCu}_2\text{O}_{8+y}$  in the absence of a pseudogap. Circles — experimental points from Ref. 16, curve — computed form.

$\langle S_i S_j \rangle_3 = 0.09$ . These values describe well the shape of the Fermi surface (Fig. 1), measured recently by photoemission methods.<sup>14,15</sup> This circumstance gives us a solid foundation for analyzing the temperature dependence of the response function and pseudogap, which, as is well known,<sup>16</sup> depend strongly on the form of the Fermi surface. Calculated by us for  $\delta = 0.33$  (Fig. 1), it agrees well with the experimental data for  $\text{Bi}_2\text{Sr}_2\text{CaCu}_2\text{O}_{8+y}$ .<sup>15</sup> The tunneling parameter  $-t_{ab} = 50$  meV was chosen on the basis of the photoemission data.<sup>14,17,18</sup>

An important feature of the bonding singlet band is that its spectral weight depends on the doping  $\delta$  as  $4\delta/(2+\delta)$  and therefore the half-filling condition holds for  $\delta = 2/7$ . This qualitatively explains the unusual behavior of the phase diagram of  $T_c$  and  $T^*$  as a function of the doping.<sup>3</sup>

A numerical calculation of the response function gave a result similar to Ref. 16. It showed that for the above-described anisotropy of the Fermi surface it has a maximum at  $Q_x = \pm \pi/a$  and  $Q_y = \pm \pi/a$ , i.e., the system of current carriers has a Peierls-type instability. The elementary excitation spectrum under such conditions is modified to the form

$$E_{1k,2k} = \frac{\epsilon_k + \epsilon_{k+Q}}{2} \pm \frac{1}{2} [(\epsilon_k - \epsilon_{k+Q})^2 + 4|G_{ph}(k, T) + G_{ex}(k, T)|^2]^{1/2}. \quad (6)$$

The equation for the phonon component of the gap,  $G_{ph}(k, T)$ , has a form characteristic for charge-density waves:<sup>8,19</sup>

$$G_{ph}(k, T) = -\frac{P_p}{N} \sum_{k_1} V_{k_1, Q} \langle \Psi_{k_1+Q}^{pd, \uparrow} \Psi_{k_1}^{\uparrow, pd} \rangle - V_{k, Q} \frac{P_p}{N} \sum_{k_1} \langle \Psi_{k_1+Q}^{pd, \uparrow} \Psi_{k_1}^{\uparrow, pd} \rangle. \quad (7)$$

The factor  $P_p$  in Eq. (7) appears because the anticommutators of the quasi-Fermi operators are different from 1;  $V_{k, Q}$  is the interaction potential via the phonon mode  $\omega_Q$ .<sup>18</sup>

$$V_{k,Q} = \frac{2|V(Q)|^2 \hbar \omega_Q}{(\hbar \omega_Q)^2 - (\epsilon_k - \epsilon_{k+Q})^2} \Theta(\hbar \omega_D - |\epsilon_k - \epsilon_{k+Q}|), \quad (8)$$

where  $\omega_D$  is the Debye frequency,  $\Theta(x)$  is the theta function, and  $V(Q)$  is a constant characterizing the interaction with the phonon mode. In Refs. 5 and 19 it was noted that the breathing mode  $\omega_D = 45$  meV of the oxygen atoms in the  $\text{CuO}_2$  planes participates most actively in the Peierls transition.

The superexchange component  $G_{ex}(k, T)$  of the gap is determined by the expression

$$G_{ex}(k, T) = -\frac{1}{P_p N} \sum_{k_1} [J(k_1 - k) + 2K(k_1 - k)] \langle \Psi_{k_1+Q}^{pd, \uparrow} \Psi_{k_1}^{\uparrow, pd} \rangle. \quad (9)$$

Here  $J(q)$  and  $K(q)$  are the Fourier transforms of the superexchange and Coulomb interactions, respectively. Specifically,  $J(q) = J_1(\cos q_x a + \cos q_y a)$ , where  $J_1$  is the superexchange coupling constant between the nearest neighbors of the copper ions in the  $\text{CuO}_2$  plane.

The temperature dependences  $G_{ph}(k, T)$  and  $G_{ex}(k, T)$  are calculated self-consistently from Eqs. (7) and (9). The correlation function  $\langle \Psi_{k+Q}^{pd, \uparrow} \Psi_k^{\uparrow, pd} \rangle$  is determined by the formula

$$\langle \Psi_{k_1+Q}^{pd, \uparrow} \Psi_{k_1}^{\uparrow, pd} \rangle = P_p \frac{G_{ph}(k, T) + G_{ex}(k, T)}{\epsilon_{1k} - \epsilon_{2k}} [f(\epsilon_{1k}) - f(\epsilon_{2k})]. \quad (10)$$

Numerical solutions of the system of equations (7) and (9) show that for the values of interest to us  $\delta = 0.1 - 0.3$  the wave-number dependence of the pseudogap function can be represented as

$$G(k, T) = A(T) + B(T) \frac{(\hbar \omega_Q)^2 \Theta(\hbar \omega_D - |\epsilon_k - \epsilon_{k+Q}|)}{(\hbar \omega_Q)^2 - (\epsilon_k - \epsilon_{k+Q})^2} + iD(T) [\cos k_x a - \cos k_y a]. \quad (11)$$

The temperature dependences  $A(T)$  and  $D(T)$  with  $|V(Q)| = 80$  meV,  $\hbar \omega_Q = 40$  meV, and  $J_1 + 2K_1 = 210$  meV are displayed in Fig. 2. The ratio  $A(T)/B(T) = 0.73$ . We note that our computed value of the critical temperature  $T_{ph}^* \approx 170$  K is identical to the onset temperature of anomalies associated with the lattice (softening of the phonon modes in the Raman spectrum,<sup>20</sup> changes in the NQR frequencies,<sup>21,22</sup> and others), which are interpreted in Ref. 19 as a manifestation of charge-density waves in the  $\text{YBa}_2\text{Cu}_4\text{O}_8$  crystal.

Figure 3 displays our computed value of the Knight shift on the Cu(2) copper nuclei in  $\text{YBa}_2\text{Cu}_4\text{O}_8$  with  $\delta = 0.29$ . The experimental data were taken from Refs. 23 and 24. The weak manifestation of  $T_{ph}^*$  is also seen in this plot. Compared with the Fermi-liquid pictures, the phase transition point is strongly masked by the temperature dependence  $G_{ex}(k, T)$ . The variance of the critical temperature on account of fluctuations is not determining in this case. In the case  $G_{ex}(k, T) = 0$ , the kink in  $K_s(T)$  at  $T_{ph}^*$  would be sharper and for  $T > T_{ph}^*$  the Knight shift would not depend on the temperature. As one can see in Fig. 3, the presence of the pseudogap  $G_{ex}(k, T)$  explains well the nontrivial temperature dependence  $K_s(T)$  in the entire temperature interval  $T > T_{ph}^*$ .

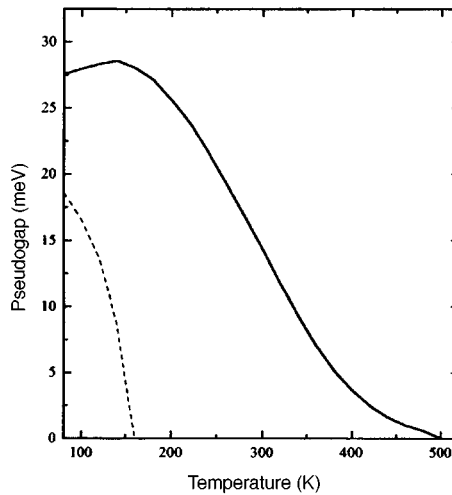


FIG. 2. Pseudogap versus temperature. Solid line —  $D(T)$ , dashed line —  $A(T)$ .

The wave-number dependence of the pseudogap (11) for  $T > T_{ph}^*$  agrees with the photoemission data<sup>1,2,25</sup> for  $\text{Bi}_2\text{Sr}_2\text{CaCu}_2\text{O}_{8+y}$ , according to which the pseudogap in the elementary excitation spectrum of the normal phase is described approximately by a formula of the form  $c(\cos k_x a - \cos k_y a)$ , i.e., it possesses  $d$ -type symmetry. As one can see from Fig. 2, this conclusion should be absolutely accurate for samples with  $T > T_{ph}^*$ , while for  $T_c < T < T_{ph}^*$  the  $s$ -type component of the pseudogap should also be easily noticeable. It would be interesting to check this prediction of the theory experimentally.

In conclusion, we note that although we have discussed in the present letter only bilayer cuprates, our conclusion that the pseudogap possesses  $s + id$  symmetry holds in general. In particular, it is valid for single- and trilayer high- $T_c$  superconductors with the corresponding degrees of doping. It is underscored in a recent investigation<sup>26</sup> of the

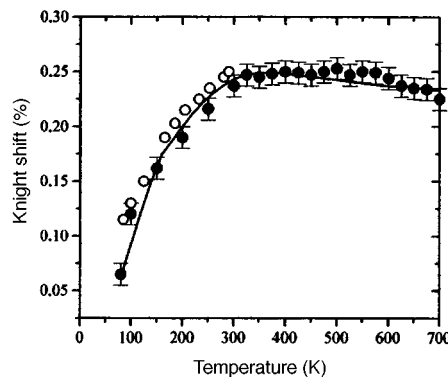


FIG. 3. Temperature dependence of the Knight shift for Cu(2) (magnetic field  $\perp z$  axis) in  $\text{YBa}_2\text{Cu}_2\text{O}_8$ . Line — computed curve, circles — experimental data (filled circles — Ref. 24, open circles — Ref. 23).

photoemission from the multilayer cuprates  $\text{Bi}_2\text{Sr}_2\text{Ca}_{1-x}\text{Dy}_x\text{Cu}_2\text{O}_{8+y}$  that the general functional dependences of the pseudogap and superconducting gap, which are proportional to  $(\cos k_x a - \cos k_y a)$ , point to a common origin. The results of the present letter are consistent with this conclusion. In Ref. 27 it is shown by solving the BCS equation numerically that any short-range potentials with Fourier transforms proportional to  $(\cos k_x a + \cos k_y a)$  (primarily superexchange between the nearest copper spins) with not very low degrees of doping will always lead to  $d$ -type pairing; in our solution for the pseudogap (and  $T_{ex}^*$ ) the  $d$  component is also the result of a short-range interaction. It is evident from Eq. (9) that in the case of a pseudogap superexchange and the screened Coulomb interaction intensify one another. In the case of a superconducting gap, however, the situation is reversed. This circumstance qualitatively explains why  $T_{ex}^*$  in underdoped cuprates is higher than  $T_c$ , even though the potential leading to their appearance is also short-ranged. This question will be discussed in greater detail in a separate paper.

S. V. V. and I. M. E. are grateful to the International Soros Science Education Program "Soros Graduate Students" (Grants Nos. a97-2930 and a97-1981) for financial support.

- <sup>1</sup>H. Ding, T. Yokoya, J. C. Campuzano *et al.*, Nature **382**, 51 (1996).
- <sup>2</sup>A. G. Loeser, Z.-X. Shen, D. S. Dessau *et al.*, Science **273**, 325 (1996).
- <sup>3</sup>G. V. M. Williams, J. L. Tallon, E. M. Haines *et al.*, Phys. Rev. Lett. **78**, 721 (1997).
- <sup>4</sup>D. Pines, *Proceedings of the Fifth International Conference on Materials and Mechanisms of Superconductivity. High-Temperature Superconductors (M<sup>2</sup>S-HTSC-V)*, Beijing, Feb. 28–Mar. 4, 1997; to be published in Physica C
- <sup>5</sup>R. S. Markiewicz, Physica C. **193**, 323 (1992); J. Phys. Chem. Solids, in press.
- <sup>6</sup>X.-G. Wen and P. A. Lee, Phys. Rev. Lett. **76**, 503 (1996).
- <sup>7</sup>V. J. Emery and S. A. Kivelson, Nature **374**, 434 (1995).
- <sup>8</sup>C. A. Balseiro and L. M. Falicov, Phys. Rev. B **20**, 4457 (1979).
- <sup>9</sup>I. Eremin and M. Eremin, J. Superconductivity **10**, 459 (1997).
- <sup>10</sup>M. V. Eremin, S. G. Solov'yanov, S. V. Varlamov *et al.*, JETP Lett. **60**, 125 (1994).
- <sup>11</sup>K. Gofron, J. C. Campuzano, H. Ding *et al.*, J. Phys. Chem. Solids **54**, 1193 (1993).
- <sup>12</sup>M. V. Eremin, S. G. Solovjanov, and S. V. Varlamov, J. Phys. Chem. Solids **56**, 1713 (1995); M. V. Eremin, S. G. Solov'yanov, and S. V. Varlamov, JETP (1997), in press.
- <sup>13</sup>N. M. Plakida, R. Hayn, and J. L. Richard, Phys. Rev. B **51** 16599 (1995).
- <sup>14</sup>M. S. Shabel, C.-H. Park, A. Matsuura *et al.*, Phys. Rev. B **55**, 2796 (1997).
- <sup>15</sup>H. Ding, N. R. Norman, T. Yokoya *et al.*, Phys. Rev. B, to be published.
- <sup>16</sup>G. Gruner, *Density Waves in Solids*, Addison-Wesley, New York, 1994.
- <sup>17</sup>Z.-X. Shen and J. R. Schrieffer, Phys. Rev. Lett. **78**, 1771 (1997).
- <sup>18</sup>M. R. Norman, H. Ding, J. C. Campuzano *et al.*, Phys. Rev. B, to be published.
- <sup>19</sup>I. Eremin, M. Eremin, S. Varlamov *et al.*, Phys. Rev. B **56**, N17 (1997).
- <sup>20</sup>A. P. Litvinchuk, C. Thomsen, and M. Cardona, Solid State Commun. **83**, 343 (1992).
- <sup>21</sup>A. Suter, D. Brinkmann, M. Mali, and J. Ross, Phys. Rev. B **8** (1997), to be published.
- <sup>22</sup>M. A. Teplov, E. V. Kryukov, A. V. Duglav *et al.*, JETP Lett. **63**, 227 (1996).
- <sup>23</sup>M. Bankay, M. Mali, J. Roos, and D. Brinkmann, Phys. Rev. B **50**, 6416 (1994).
- <sup>24</sup>N. J. Curro, T. Imai, C. P. Slichter, and B. Dabrowski, Phys. Rev. B **56**, 877 (1997).
- <sup>25</sup>J. M. Harris, Z. X. Shen, P. J. White *et al.*, Phys. Rev. B **54**, 15665 (1996).
- <sup>26</sup>J. M. Harris, P. J. White, Z.-X. Shen *et al.*, Phys. Rev. Lett. **79**, 499 (1997).
- <sup>27</sup>M. Eremin and I. Larionov, JETP Lett. **62**, 203 (1995).

Translated by M. E. Alferieff

# Magnetoplasmon replica in the recombination radiation spectra of a quasi-two-dimensional electron gas in GaAs/AlGaAs quantum wells

O. V. Volkov,<sup>a)</sup> V. E. Zhitomirskiĭ, and I. V. Kukushkin

*Institute of Solid State Physics, Russian Academy of Sciences, 142432 Chernogolovka, Moscow Region, Russia*

K. von Klitzing and K. Eberl

*Max-Planck-Institut für Festkörperforschung, 70569 Stuttgart, Germany*

(Submitted 12 September 1997)

*Pis'ma Zh. Éksp. Teor. Fiz.* **66**, No. 8, 539–544 (25 October 1997)

The radiative recombination spectra of two-dimensional electrons with free photoexcited holes are investigated for a wide variety of GaAs/AlGaAs quantum wells, with different thicknesses and electron densities. It is found that for certain, close to integral, filling factors an intense line corresponding to an Auger process — radiative recombination with the emission of an additional magnetoplasmon — appears in the luminescence spectrum. The new line is shifted to lower energies with respect to the zero Landau level, and the magnetic field dependence of the energy splitting between these lines agrees with the theoretical concepts of the dispersion of magnetoplasmon excitations. This makes it possible to estimate the magnetoplasmon energy at the roton minimum. © 1997 American Institute of Physics.

[S0021-3640(97)00620-8]

PACS numbers: 73.20.Dx, 73.20.Mf, 78.60.–b, 78.55.Cr

1. Interest in two-dimensional (2D) electron systems has increased substantially in recent years. This is due not only to the diverse potential applications of such systems in microelectronics but also the discovery of new fundamental physical phenomena — the integral and fractional quantum Hall effects (QHEs).<sup>1</sup> These phenomena are specific to 2D systems, and in order to understand them at the microscopic level it is necessary to know the structure of the elementary excitation spectrum of a system of 2D electrons in a perpendicular magnetic field. It is known that the dispersion of such excitations is determined by the electron–electron interaction, which dominates at wavelengths comparable to the characteristic interparticle distance. The electron–electron interaction determines the dispersion of spin density waves in the QHE, the magnetoroton gap in the fractional QHE, the magnetophonon spectrum in a Wigner crystal, and the renormalization of the magnetoplasmon spectrum. As follows from the law of quasimomentum conservation in radiative recombination, the standard optical methods, based on the study of the radiative recombination of 2D electrons with free photoexcited holes, yield information about the quasiparticle dispersion only in the long-wavelength region of the spectrum. For this reason, Auger recombination processes could be effective for investi-

gating the short-wavelength part of the excitation spectrum, since the participation of an additional recoil particle makes it possible to overcome the restrictions due to the law of quasimomentum conservation. An example of processes of this kind is electron–hole recombination with the excitation of a magnetoplasmon — a collective excitation consisting of an electron in one Landau level and a “hole” in another, coupled by the Coulomb interaction.<sup>2</sup> As was shown in Ref. 3, magnetoplasmon excitation can influence the shape of the spectrum accompanying resonance crossing of optical transitions and even results in the appearance of new lines in the spectrum — magnetoplasmon replicas shifted to lower energies by the amount of the magnetoroton energy.<sup>4</sup> It should be noted that Auger processes have been observed in similar samples by many authors and attributed to either transfer processes accompanying recombination of multiparticle excitonic complexes<sup>5</sup> or emission of optical phonons accompanying recombination of electrons from high-lying Landau levels.<sup>6</sup> For this reason, to attribute unequivocally a replica, which we were the first to observe in Ref. 4, to the excitation of magnetoplasmons it is necessary to study the magnetic field dependence of the energy splitting in a wide range of 2D-electron densities. We investigated the 2D-electron luminescence spectrum of a family of asymmetrically doped 200, 250, 300, and 350 Å thick quantum wells with carrier density  $n_s$  ranging from  $1.6 \times 10^{11} \text{ cm}^{-2}$  to  $6.1 \times 10^{11} \text{ cm}^{-2}$  and mobility  $\mu$  ranging from  $3 \times 10^5$  to  $9 \times 10^5 \text{ cm}^2/\text{V}\cdot\text{s}$ . We observed a magnetoplasmon replica in all experimental structures. The replica demonstrated properties which are common to all samples — the line is excited under conditions close to a QHE regime and the energy splitting corresponding to the excitation of a magnetoplasmon manifests a square-root dependence on the magnetic field, i.e., it is proportional to the Coulomb interaction energy at a distance of the order of the magnetic length. This confirms the conjecture that the appearance of the replica is due to the excitation of magnetorotons.

2. A series of seven high-quality, asymmetrically doped, single quantum wells was grown by molecular-beam epitaxy on GaAs substrates (see Ref. 4). Optical excitation of the system was performed with a tunable Ti/Sp laser. A U-1000 Ramanor double monochromator served as a spectrometer. Combined with a CCD detector, it gave a resolution of 0.03 meV. The density and mobility of the 2D-electron gas were measured by transport methods on the same structure under laser illumination conditions. Weak illumination of the system with a He/Ne laser was used for additional control of the electron density. The experiments were conducted at a temperature of 1.5 K in magnetic fields ranging from 0 to 11 T and directed perpendicular to the plane of the quantum wells.

3. Fragments of the luminescence spectra corresponding to the recombination of 2D electrons in the zero Landau level are displayed in Fig. 1. The spectra were measured for a 250 Å thick quantum well with carrier density  $n_s = 3.9 \times 10^{11} \text{ cm}^{-2}$  in different magnetic fields in  $\sigma$  polarization. The strongest transition in the spectrum of the zero Landau level is a transition between the lowest energy levels of the electrons and heavy holes  $0 + 0h+$  (the high-energy line in Fig. 1). However, as one can see from Fig. 1, for certain filling factors, specifically, in the region  $\nu \approx 2.3$  (a) and  $\nu \approx 4.3$  (b), a pronounced wide line appears on the low-energy edge of the zero Landau level. As noted in Ref. 4, this line is due to the excitation of a magnetoplasmon in an electron–hole recombination process. Figure 1c shows the ratio of the intensities of the magnetoplasmon replica and the main transition  $0 + 0h+$  as a function of the filling factor. As one can see from the figure, the

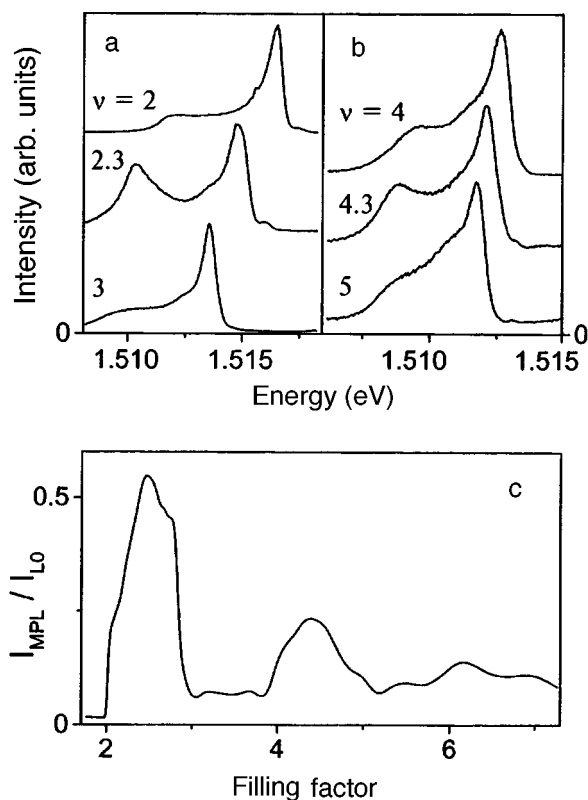


FIG. 1. (a, b) Radiative recombination spectra of 2D electrons in the zero Landau level. The spectra were measured for a 250 Å thick well with carrier density  $n_s = 3.9 \times 10^{11} \text{ cm}^{-2}$  in different magnetic fields corresponding to the indicated filling factors. (c) The relative intensity of magnetoplasmon replica versus the filling factor.

magnetoplasmon replica appears in the ranges  $2 < \nu < 3$  and  $4 < \nu < 5$  with maxima at  $\nu \approx 2.3$  and  $4.3$ .

The reasons for such behavior must be sought in the selection rules for optical transitions. As is well known, the main allowed electron–hole transitions are transitions between electron and hole Landau levels with the same numbers ( $N_e = N_h$ ). Transitions between levels with different numbers ( $N_e \neq N_h$ ) have a much lower amplitude.<sup>7,8</sup> However, since the photoexcited-hole density in the system is very low, in the process of energy relaxation virtually all holes are in the lowest energy level  $0h+$ . As a result, the luminescence intensity of Landau levels with  $N_e > 0$  drops off rapidly with increasing level number. However, recombination of electrons from a Landau level with  $N_e > 0$  and holes from the level  $0h+$  is nonetheless possible, if it is accompanied by excitation of a magnetoplasmon which carries off the uncompensated angular momentum, equal to  $N_e$ . The spin selection rules allow only a transition with the participation of the lowest spin sublevel  $N_e+$ , polarized in  $\bar{\sigma}$  polarization. The magnetoplasmon participating in this

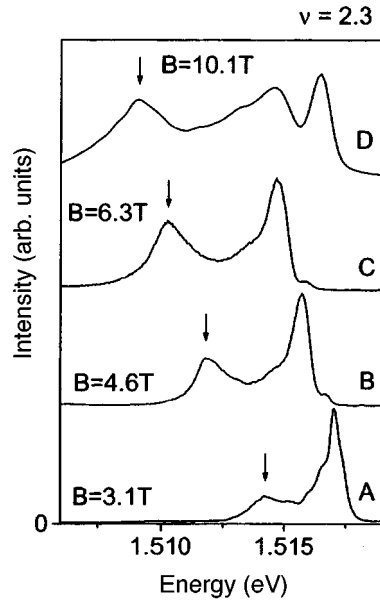


FIG. 2. Luminescence spectra of the zero Landau level. The spectra were obtained for four 250 Å thick quantum wells with carrier densities  $n_s = 1.7 \times 10^{11}$ ,  $2.6 \times 10^{11}$ ,  $3.5 \times 10^{11}$ , and  $5.6 \times 10^{11} \text{ cm}^{-2}$  (A, B, C, and D, respectively) in magnetic fields corresponding to filling factor  $\nu = 2.3$ . The arrows mark magnetoplasmon replicas.

process is a pair consisting of an electron in an empty or partially-filled Landau level and a “hole” in a completely filled Landau level, the level numbers differing by  $\Delta N = N_e$ , with energy  $\Delta N \cdot \hbar \omega_c + \Delta E(k)$ . On the basis of Kohn’s theorem,<sup>9</sup> when only the electron–electron interaction is taken into account the total momentum of such a pair is  $k = 0$  and the excitation energy is  $\Delta N \cdot \hbar \omega_c$  (since  $\Delta E(0) = 0$ ). This means that the energy of the emitted photon is shifted exactly by  $N_e \hbar \omega_c$ , i.e., it equals the energy of the photon emitted in the recombination  $0 + 0h+$ . However, taking account of the interaction of the 2D electrons with distant ionized donors in the doped layer can substantially alter the picture described above. It is known that under integral QHE conditions, when the filling factor is only slightly greater than an even number, all electrons in the upper Landau level are localized on fluctuations of the random potential<sup>1</sup> with size of the order of the magnetic length  $l_H = (\hbar c / eB)^{1/2}$ . As a result of the recombination of such electrons accompanied by excitation of magnetoplasmons, the latter acquire a quasimomentum of the order of  $k \sim 1/l_H$  and the photon energy is shifted by  $\Delta E(k)$  relative to the energy of the transition  $0 + 0h+$ . Therefore a low-energy tail of the recombination spectrum of the zero Landau level is formed. Its specific form is completely determined by the magnetoplasmon density of states, i.e., it depends on the magnetoplasmon dispersion relation. As is well known, the magnetoplasmon dispersion relation<sup>2</sup> has a pronounced minimum near quasimomenta of the order of the reciprocal  $1/l_H$  of the magnetic length. The energy corresponding to this minimum is proportional to the Coulomb interaction energy  $\Delta E \sim e^2 / \epsilon l_H$  at a distance of the order of the magnetic length. The corresponding maxi-

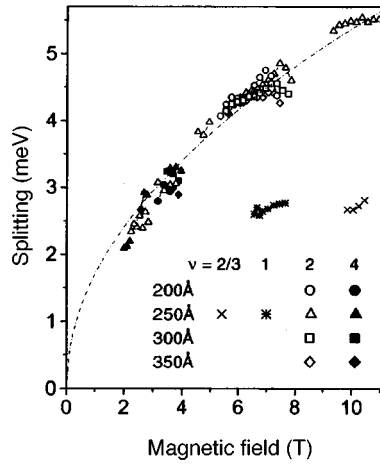


FIG. 3. Magnetic field dependence of the energy splitting between a line corresponding to a  $0 + 0h+$  transition and a magnetoplasmon replica, measured for wells with different thicknesses and 2D-electron densities. Inset: Correspondence between the parameters and the symbols employed in the plot. The dot-dash line corresponds to the Coulomb energy at the magnetic length with proportionality coefficient corresponding to the experimental data.

imum in the density of states should lead to the appearance of a line split off by an amount equal to the magnetoplasmon energy at the minimum (magnetorotons). The intensity of this line with small deviations from an even filling factor should grow as the number of electrons in the upper Landau level. As the filling factor increases further and the average distance between the electrons in the upper Landau level becomes comparable to the magnetic length  $l_H$ , the electrons start to screen effectively the fluctuations of the random potential. As a result, the intensity of the magnetoplasmon replica decreases because the number of localized electron states decreases. We note that the creation of a magnetoplasmon with a nonzero quasimomentum in the process of recombination of a 2D electron from a completely filled Landau level (below the Fermi surface) is impossible because of the uniform electron density distribution.<sup>10</sup>

In summary, the filling factor dependence of the relative intensity of the magnetoplasmon replica, presented in Fig. 1c, agrees completely with the above-described mechanism leading to the appearance of the replica. Moreover, this mechanism also makes it possible to explain the extinction, which we observed in Ref. 4, of the magnetoplasmon replica with increasing temperature on account of the thermal delocalization of the electrons.

To confirm the relation between the replica, which we observed, and the excitation of magnetorotons, we investigated the dependence of the energy splitting between the magnetoplasmon replica and the main transition  $0 + 0h+$  for the zero Landau level. Figure 2 shows the spectra for four different 2D-electron densities in magnetic fields corresponding to filling factor  $\nu = 2.3$  for a 250 Å thick quantum well. The arrow marks the position of the magnetoplasmon replica. The magnetic field dependence of the energy splitting for all experimental samples is shown in Fig. 3. The different symbols in the

figure represent different combinations of the well thickness and filling factor; the inset shows the correspondence. In each case the points were plotted in a magnetic field range where the magnetoplasmon replica is pronounced:  $2 < \nu < 3$  for  $\nu=2$  dots and  $4 < \nu < 5$  for  $\nu=4$  dots. As one can see from the figure, irrespective of the thickness of the quantum well and electron density, all dots corresponding to the excitation of a cyclotron magnetoplasmon ( $\nu=2, 4$ ) fall on the same universal curve, which is very close to a square-root law (dot-dash line in Fig. 3). The coefficient of this curve  $\delta E \approx 0.38e^2/\epsilon l_H$  is somewhat larger than the magnetoroton energy  $0.25e^2/\epsilon l_H$  calculated in Ref. 2 with  $\Delta N=1$ .

A magnetoplasmon replica was also observed for two 250 Å thick quantum wells near the filling factor  $\nu=1$ , which corresponds to the excitation of spin-density waves. The coefficient in the square-root approximation  $\delta E \approx 0.22e^2/\epsilon l_H$  is found to be in reasonable agreement with the value  $0.15e^2/\epsilon l_H$  computed in Ref. 2. For one of these samples with a 250 Å thick well, a magnetoplasmon replica with  $\delta E \approx 0.19e^2/\epsilon l_H$  was also found near the filling factor  $\nu=2/3$  (Fig. 3). In the case at hand, magnetoplasmons can arise in a system of composite fermions ( $\nu^*=2$ ). A separate theoretical investigation is required in order to determine the dispersion relation for the collective excitations in this case.

**4.** In summary, we have shown that a magnetoplasmon replica appears in the low-energy tail of the zero Landau level when the filling factor is only slightly greater than an even number. This corresponds to the excitation of a cyclotron magnetoplasmon with nonzero quasimomentum in the process of recombination of electrons in a partially-filled upper Landau level with holes in the lowest energy level. The magnetic-field dependence of the energy splitting confirms that this replica is due to the additional minimum in the dispersion relation for magnetoplasmons at  $k \approx 1/l_H$ , and the coefficient of this dependence is in reasonable agreement with theoretical calculations. Magnetoplasmon replicas were also observed near filling factors  $\nu=1$  and  $\nu=2/3$ . They could be associated with the excitation of spin-density waves and magnetoplasmons in a system of composite fermions.

This work was supported by the Russian Fund for Fundamental Research (Grant 96-02-16177) and INTAS (Grant 95-IN/RU-675).

<sup>a)</sup>e-mail: volkov@issp.ac.ru

<sup>1</sup>R. E. Prange and S. M. Girvin, *The Quantum Hall Effect*, Springer, New York, 1990.

<sup>2</sup>C. Kallin and B. I. Halperin, *Phys. Rev. B* **30**, 5655 (1984).

<sup>3</sup>L. V. Butov, L. V. Kulik, V. D. Kulakovskii, and T. G. Andersson, *JETP Lett.* **56**, 557 (1992).

<sup>4</sup>O. V. Volkov, V. E. Zhitomirskii, I. V. Kukushkin *et al.*, *JETP Lett.* **65**, 38 (1997).

<sup>5</sup>G. Finkelstein, H. Shtrikman, and I. Bar-Joseph, *Phys. Rev. B* **53**, 12593 (1996).

<sup>6</sup>P. E. Simmonds *et al.*, *Surf. Sci.* **263**, 646 (1992).

<sup>7</sup>C. R. Pidgeon and R. N. Brown, *Phys. Rev.* **146**, 575 (1966).

<sup>8</sup>B. B. Goldberg *et al.*, *Phys. Rev. B* **38**, 10131 (1988).

<sup>9</sup>W. Kohn, *Phys. Rev.* **123**, 1242 (1961).

<sup>10</sup>B. Janovici, *Phys. Rev. Lett.* **46**, 386 (1981).

Translated by M. E. Alferieff

# On the electrostatic potential distribution in a screened Corbino disk carrying a transport current under conditions of the quantum Hall effect

V. B. Shikin

*Institute of Solid State Physics, Russian Academy of Sciences, 142432 Chernogolovka, Moscow Region, Russia*

(Submitted 3 July 1997; resubmitted 18 September 1997)

*Pis'ma Zh. Eksp. Teor. Fiz.* **66**, No. 8, 545–550 (25 October 1997)

It is shown that the characteristic features of the chemical potential for 2D electrons in a magnetic field, which lead to sharp dips in the magnetic field dependence of the capacitance of a 2D system, also affect the electrostatic potential distribution in the direction of the transport current flowing through a 2D Corbino disk under conditions of integral magnetic filling factor. The associated details of the temperature dependence of the electrostatic potential distribution, the distances to the screening electron, and the transport potential difference at the Corbino edges are investigated. The possibilities of experimentally observing these features of the electrostatic potential distribution along a Corbino disk with a transport current under conditions of the quantum Hall effect are discussed. © 1997 American Institute of Physics. [S0021-3640(97)00720-2]

PACS numbers: 73.20.Dx, 73.40.Hm

Measurements of the conductance of a two-dimensional Corbino disk in a normal magnetic field are basic measurements yielding the most accurate information about the diagonal part of the conductance of an experimental 2D system in a magnetic field. It is obvious that the computed part of the conductance of a Corbino disk must be as accurate as possible in order adequately to extract the desired conductivity from the experimental data. In this connection, as well as for reasons of independent interest, the present letter discusses a number of features of “chemical” origin in the radial electrostatic potential distribution in a Corbino disk carrying a transport current.

It is well known that the quantum Hall effect (QHE) in 2D-electron systems and the deep dips deep in the minima of the magnetocapacitance of such media are related. The presence of dips in the magnetocapacitance is due to the characteristic features of the electrochemical potential  $\mu$  of 2D electrons in a magnetic field.<sup>1</sup> On the other hand, the QHE is ordinarily associated with the properties of the conductivity tensor.<sup>2</sup> But the diagonal electron current density  $j_i$  is proportional to both the conductivity  $\sigma_{ii}$  and the gradient of the electrochemical potential  $\mu$

$$j_i = e^{-1} \sigma_{ii} \partial \mu / \partial x_i. \quad (1)$$

Therefore it is natural to conjecture that the transport problem should exhibit characteristic features at integral filling factors not only for the current density itself (1) but also

for the combination

$$j_i/\sigma_{ii}=e^{-1}\partial\mu/\partial x_i. \quad (1a)$$

The results presented below confirm this conjecture. Specifically, we consider the problem of the appearance of a spatial nonuniformity in the radial distribution of the electrochemical potential in a Corbino disk. The details of this nonuniformity are very sensitive to the external parameters: temperature, closeness of the equilibrium filling factor to an integer, degree of screening of the disk, and so on. Significantly, such local details are now accessible to observation, for example, by means of the linear electrooptic effect,<sup>3-5</sup> which is employed systematically for studying different local electrostatic potential distributions in a 2D-electron system, or by different versions of Kelvin's local capacitance method (see Refs. 6 and 7).

Let us consider a standard 2D-electron system in the form of a Corbino disk with inner and outer radii  $R_0$  and  $R_1$ , respectively. The system is covered by a controlling electrode located at a distance

$$d\ll(R_1-R_0). \quad (2)$$

For the geometry employed, it is convenient to rewrite Ohm's law (1a) as

$$J/2\pi r=e^{-1}\sigma_{rr}d\mu/dr, \quad 0\leq\mu\leq V, \quad V\leq V_{cr}. \quad (3)$$

Here  $J$  is the total radial current, which is maintained at a fixed value, in the sample;  $\sigma_{rr}$  is the diagonal part of the conductivity, which depends in a definite manner on the characteristics of the 2D system, the temperature  $T$ , and the magnetic field  $H$  but does not depend on  $d\mu/dr$  and, by definition, is uniform over the 2D system;  $V$  is the transport potential difference maintained at the edges of the Corbino disk; and,  $V_{cr}$  is the critical potential difference corresponding to breakdown of the QHE in the sample. In the literature there is still no unanimity about the distribution of  $V_{cr}$  (see references cited in Refs. 8-13), though ingenious work<sup>8</sup> on the breakdown of the QHE shows that

$$T\ll eV_{cr}\leq\hbar\omega_c, \quad (4)$$

where  $\omega_c$  is the cyclotron frequency.

It follows from Eq. (3) that the local value of the electrochemical potential along a Corbino disk equals

$$\mu(r)=\mu_0+\frac{eJ}{2\pi\sigma_{rr}}\ln\left(\frac{r}{R_0}\right), \quad R_1>r>R_0. \quad (5)$$

The current  $J$  is related with the potential difference  $V$  on the metallic edges of the Corbino disk,  $\mu(R_1)-\mu(R_0)=V$  and  $\mu(R_0)\equiv\mu_0$ , so that

$$\frac{eJ}{2\pi\sigma_{rr}}\ln\left(\frac{R_1}{R_0}\right)=V. \quad (6)$$

As a result, expression (5) can be rewritten in a form that does not depend on  $\sigma_{rr}$ :

$$\mu(r)-\mu_0=V\ln\left(\frac{r}{R_0}\right)\bigg/\ln\left(\frac{R_1}{R_0}\right). \quad (7)$$

The electrochemical potential distribution (7) is a continuous monotonic function of  $r$ .

Proceeding now to determining the electrostatic potential distribution  $\varphi(r)$  and the electron density  $n(r)$ , we write out an explicit relation between  $\mu(r)$ ,  $\varphi(r)$ , and  $n(r)$  for an ideal 2D-electron system in a magnetic field. Under conditions when the filling factor  $\nu$  does not exceed 2 ( $\nu < 2$ ) and the spin splitting can be neglected, this relation has the form

$$\mu(r) = e\varphi(r) - T \ln S(H, T, \nu(r)), \quad (8)$$

where

$$2S(H, T, \nu) = \left(\frac{1}{\nu} - 1\right) + \left[\left(\frac{1}{\nu} - 1\right)^2 + 4\epsilon\left(\frac{2}{\nu} - 1\right)\right]^{1/2},$$

$$\epsilon = \exp(-\hbar\omega_c/T) \ll 1, \quad \nu < 2,$$

$$\nu(r) = \pi l_h^2 n(r), \quad l_h^2 = c\hbar/eH. \quad (9)$$

Near  $\nu=1$  the term  $T \ln S(\nu)$  makes the main contribution to the right-hand side of expression (8) for  $\mu$ , because here it undergoes a  $T$ -independent jump (the temperature influences only the degree of broadening of the jump) from zero to  $-T \ln S(\nu) \cong \hbar\omega_c$ . Under these conditions

$$\mu(r) - \mu_0 \cong T \ln \left[ \frac{S(H, T, \nu_0)}{S(H, T, \nu(r))} \right], \quad \nu_0 < \nu(r) \ll 1, \quad \mu(r) - \mu_0 < \hbar\omega_c \quad (8a)$$

and the gradient of the electrochemical potential is mainly of a diffusion origin (the electric field does not make a direct contribution).

The equations (7) and (8) are supplemented by Poisson's equation, which relates the electrostatic potential with the local electron density distribution. In problems with deep screening, i.e., under the conditions (2), this relation, which in the general case is an integral relation, simplifies because the so-called capacitor approximation becomes valid:

$$\varphi(r) \cong 2ed\nu(r)/kl_h^2, \quad (10)$$

where the distribution  $\varphi(r)$  (9) in the direction of the current is locally related with the local value of the filling factor  $\nu(r)$ .

Combining expressions (7), (8), and (10), we obtain finally the following dimensionless expression for  $\nu(r)$ :

$$\nu \frac{\ln x}{\ln 4/3} = 2d_*(\nu - \nu_0) - t \ln[S(\nu)/S(\nu_0)], \quad (11)$$

$$\nu = eV/\hbar\omega_c, \quad d_* = d/a_b^*, \quad t = T/\hbar\omega_c, \quad x = r/R_0, \quad R_1/R_0 = 4/3.$$

The ratio  $R_1/R_0=4/3$  in Eqs. (11) was chosen in accordance with the parameters given in Ref. 5 for a Corbino sample.

As long as the filling factor is far from an integer, the diffusion contribution to the distribution  $\nu(x)$  is very small:

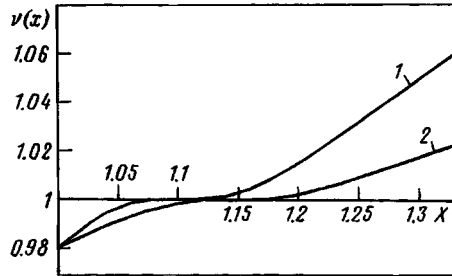


FIG. 1.  $\nu(x)$  for  $\nu = 1.5$ ,  $t = 0.05$ ,  $\nu_0 = 0.98$ , and  $d_* = 10$  (curve 1),  $d_* = 5$  (curve 2).

$$\nu \frac{\ln x}{\ln 4/3} \cong 2d_*(\nu - \nu_0), \quad |1 - \nu_0| \gg t. \quad (11a)$$

However, the situation changes qualitatively if  $\nu_0 \approx 1$ . Here

$$\nu \frac{\ln x}{\ln 4/3} \cong -t \ln[S(\nu)/S(\nu_0)], \quad |1 - \nu_0| \leq t. \quad (11b)$$

Under the conditions

$$t \ll \nu \ll \nu_{cr} \quad (12)$$

a plateau appears in the function  $\nu(x)$  at the location where the local filling factor passes through its integral value. In the opposite limiting case

$$\nu \leq t, \quad (12a)$$

the filling factor and hence the electrostatic potential remain virtually constant along the Corbino disk (the indicated plateau fills the entire Corbino disk because  $\varphi(x) \ll \nu$ ).

Typical plots of  $\nu(r/R_0)$  from Eq. (11) are displayed in Figs. 1–4. It is easy to see that the distribution  $\nu(r)$  possesses the above-mentioned characteristic coordinate plateaus which are absent in the classical distribution  $\nu(r)$  (11a) and are sensitive to the temperature, the spacer thickness, and the value of  $\nu$ .

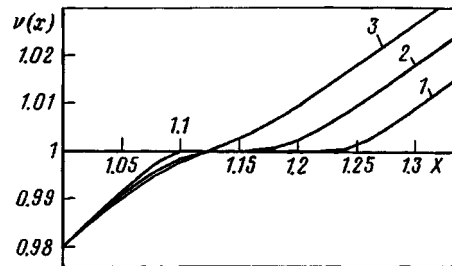


FIG. 2.  $\nu(x)$  for  $\nu = 1.5$ ,  $d_* = 10$ ,  $\nu_0 = 0.98$  and  $t = 0.025$  (curve 1),  $t = 0.05$  (curve 2),  $t = 0.075$  (curve 3).

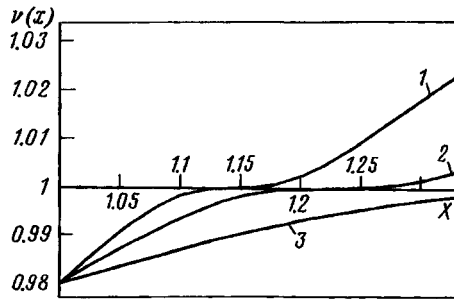


FIG. 3.  $\nu(x)$  for  $d_* = 10$ ;  $t = 0.05$ ;  $\nu_0 = 0.98$  and  $v = 1.5$  (curve 1),  $v = 1.0$  (curve 2), and  $v = 0.5$  (curve 3).

It should be underscored that the plateaus, which are displayed in Figs. 1–4, in the electrostatic potential distribution or the electron density are of the same origin as the incompressible regions discussed in Refs. 14 and 15. The difference lies only in the fact that in Refs. 14 and 15 the plateaus arise under equilibrium conditions on sections with a nonuniform electron density at locations where the filling factor locally has an integral value. In the transport problem, a disturbance produced in the electron density by a transport current flowing through a system with an integral filling factor plays the role of a spatial nonuniformity. The density gradients are much “softer,” and they are more easily observed by the different local methods mentioned above than in equilibrium problems.

We note that the case investigated in this letter is only an ideal 2D system. The temperature plays the role of a broadening factor. This simplification is compelled for technical reasons, because in the case of a finite density of states at a Landau level it is impossible to suggest for the electrochemical potential an analytic expression similar to Eqs. (8) and (8a). Nonetheless, such an approximation makes sense physically and it is productive. An entire theory of the magnetocapacitance of 2D systems, which is adequate for existing experiments, has been constructed with the aid of this approximation. Furthermore, the question of incompressible strips for the problem of a nonuniform electron system in a magnetic field can likewise be solved only for an ideal electron system (see the references cited in Refs. 14 and 15 and their many elaborations).

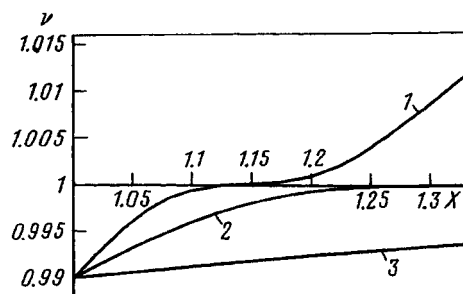


FIG. 4.  $\nu(x)$  for  $d_* = 10$ ;  $t = 0.05$ ;  $\nu_0 = 0.99$  and  $v = 1.0$  (curve 1),  $v = 0.5$  (curve 2), and  $v = 0.1$  (curve 3).

This is an opportune point at which to make a few remarks about Refs. 12 and 13. In Ref. 12, where a Corbino disk with a screening electrode was studied, the existence of spatial filamentation of the Hall current, a nonlinear effect arising under conditions which are typical for breakdown of the QHE, i.e.,  $eV \geq \hbar \omega_c$ , where  $V$  is the transport potential difference between the edges of the Corbino sample, was demonstrated experimentally. The authors attributed the filamentation effect to the appearance of an exponential dependence of the diagonal part of the conductivity on  $V$  under conditions close to breakdown of QHE. Formally the problem is to solve for the electrostatic potential an equation arising from the requirement that the radial component of the transport electric current be stationary, written in the form (3) with  $\partial\varphi/\partial r$  instead of  $\partial\mu/\partial r$ :

$$J/2\pi r = e^{-1} \sigma_{rr}(\varphi) d\varphi/dr, \quad 0 \leq \mu \leq V, \quad (13)$$

and  $\sigma_{rr}(\varphi)$  is the diagonal part of the conductivity, which depends on the local transport electrostatic potential  $\varphi$  in the manner proposed in Ref. 12:

$$\sigma_{rr} \propto \exp(+e\varphi/2T). \quad (13a)$$

In order for Eq. (13a) to be valid, the 2D system must be screened, in which case the local relation (10) between the electrostatic potential and the electron density makes sense.

A similar problem without a screen, when the continuity equation for the current (Eq. (13)) remains valid but the definition of  $\sigma_{rr}(\varphi)$  (Eq. (13a)) changes, was investigated theoretically in Ref. 13.

Comparing the definitions (3) with Eqs. (13) and (13a) gives a clear picture of the difference between the questions discussed in the present letter and in Refs. 12 and 13. In our case, the limit  $V \ll V_{cr}$ , when no nonlinearities appear in the conductivity tensor as a function of the external field, was investigated. All spatial nonuniformities presented in Figs. 1–4 are related with the properties of the electrochemical potential  $\mu$  (8) near integral values of the filling factor and, in principle, are manifested for arbitrarily small values of the transport current.

Calculations of the current–voltage (I–V) characteristics<sup>12,13</sup> take account of the nonlinearity in determining the conductivity tensor at  $V \cong V_{cr}$ , where  $V_{cr}$  is determined from Eq. (4). Naturally, they are applicable in a wider range, aspiring to nonlinear effects. But the diffusion contribution to the current density, already quite noticeable at the linear stage, is dropped (the current from Eq. (13) is proportional to  $d\varphi/dr$  and not  $d\mu/dr$ ). In the general case, the validity of the simplifications from Refs. 12 and 13 is not obvious, and their quantitative validity must be checked by solving anew the problem (13) and (13a) with  $d\mu/dr$  instead of  $d\varphi/dr$ . This program has not yet been implemented.

In summary, the present letter presents a description of the characteristic features of the spatial distribution of the electrostatic potential in a Corbino disk with an Ohmic transport current under conditions of integral filling factor. Local methods for determining the electrostatic potential in a 2D system (see Refs. 3–7) make it possible to study separately how the I–V characteristics are affected by the characteristic features of the electrochemical potential on the Hall plateaus, described above, and by the nonlinearities in the conductivity tensor, which were observed in Refs. 12 in a study of the I–V

characteristics under QHE breakdown conditions. It is important to investigate both contributions from the standpoint of self-consistency of the main results in the theory of magnetotransport in 2D-electron systems.

We thank V. F. Gantmakher and V. T. Dolgoplov for a discussion of the results obtained.

This work is partially supported by the Russian Fund for Fundamental Research (Grant 96-02-19568) and INTAS (Grant 93-933).

- <sup>1</sup>T. Ando, A. B. Fowler, and F. Stern, *Rev. Mod. Phys.* **54**, 437 (1982).
- <sup>2</sup>K. von Klitzing, G. Dorda, and M. Pepper, *Phys. Rev. Lett.* **45**, 494 (1980).
- <sup>3</sup>P. F. Goutein, P. Hendriks, F. A. P. Blom *et al.*, *Surf. Sci.* **963**, 91 (1992).
- <sup>4</sup>R. Knott, W. Dietsche, K. von Klitzing *et al.*, *Semicond. Sci. Technol.* **10**, 117 (1995).
- <sup>5</sup>W. Dietsche, K. von Klitzing, and U. Ploog, *Surf. Sci.* **361**, 289 (1996).
- <sup>6</sup>Lord Kelvin, *Philos. Mag.* **46**, 82 (1898).
- <sup>7</sup>R. Steinke, M. Hoffman, M. Bohmisch *et al.*, *Appl. Phys. F* **64**, 19 (1997).
- <sup>8</sup>G. Ebert, K. von Klitzing, K. Ploog, and C. Weiman, *J. Phys.* **16**, 5441 (1983).
- <sup>9</sup>M. Cage, R. Dsiuba, B. Field *et al.*, *Phys. Rev. Lett.* **51**, 1374 (1983).
- <sup>10</sup>S. Komiyama, T. Takumasu, S. Hiyamizy, and S. Sasa, *Solid State Commun.* **54**, 479 (1985).
- <sup>11</sup>V. Pudalov and S. Semenchinskiĭ, *JETP Lett.* **42**, 232 (1985).
- <sup>12</sup>A. A. Shashkin, V. T. Dolgoplov, and S. I. Dorozhkin, *Zh. Éksp. Teor. Fiz.* **91**, 1897 (1986) [*Sov. Phys. JETP* **64**, 1124 (1986)].
- <sup>13</sup>M. I. Dyakonov and F. G. Pikus, *Solid State Commun.* **83**, 413 (1992).
- <sup>14</sup>D. B. Chklovskii, B. I. Shklovskii, and L. I. Glazman, *Phys. Rev. B* **46**, 4026 (1992).
- <sup>15</sup>D. B. Chklovskii, K. A. Matveev, and B. I. Shklovskii, *Phys. Rev. B* **47**, 12 605 (1993).

Translated by M. E. Alferieff

# Anisotropic momentum transfer in low-dimensional electron systems in a magnetic field

O. V. Kibis<sup>a)</sup>

*Novosibirsk State Technical University, 630092 Novosibirsk, Russia*

(Submitted 28 August 1977; resubmitted 22 September 1997)

*Pis'ma Zh. Éksp. Teor. Fiz.* **66**, No. 8, 551–555 (25 October 1997)

In low-dimensional systems with an asymmetric quantizing potential, an asymmetric electron energy spectrum  $\varepsilon(\mathbf{p}) \neq \varepsilon(-\mathbf{p})$ , where  $\mathbf{p}$  is the electron momentum, arises in the presence of a magnetic field. A consequence of such an energy spectrum is that momentum transfer to the electron system in mutually opposite directions in the presence of an external perturbation is different. Therefore, in the presence of a standing electromagnetic wave momentum is transferred from the wave to the electrons, which gives rise to a new type of electromotive force.

© 1997 American Institute of Physics. [S0021-3640(97)00820-7]

PACS numbers: 73.20.Dx

Consider a two-dimensional (2D) electron system in the coordinates  $\{x, y, z\}$ , where the  $z$  axis is perpendicular to the plane of the two-dimensional layer. Let the magnetic field  $\mathbf{H}$  be oriented along the  $y$  axis and let the vector potential  $\mathbf{A}$  be of the form  $A_x = Hz$ ,  $A_y = A_z = 0$ . Then the Hamiltonian of the electron is

$$\hat{\mathcal{H}} = \frac{1}{2m} \left[ \left( \hat{p}_x + \frac{eHz}{c} \right)^2 + \hat{p}_y^2 + \hat{p}_z^2 \right] + U(z), \quad (1)$$

where  $m$  is the electron effective mass,  $e$  is the modulus of the electron charge,  $U(z)$  is the quantizing potential of the 2D system, and the electron wave function is

$$\psi_k = C \varphi(k_x, z) \exp(ik_x x + ik_y y) \exp(-i\varepsilon_k t/\hbar), \quad (2)$$

where the normalization constant

$$C = \left( L_x L_y \int_{-\infty}^{\infty} |\varphi(k_x, z)|^2 dz \right)^{-1/2},$$

$L_x$  and  $L_y$  are the dimensions of the 2D system,  $\mathbf{k}$  is the electron wave vector, and  $\varepsilon_k$  is the electron energy. Substituting expression (2) into the Schrödinger equation with the Hamiltonian (1) gives

$$-\frac{\hbar^2}{2m} \frac{\partial^2 \varphi(k_x, z)}{\partial z^2} + \left[ \frac{\hbar^2 k_x^2}{2m} + \frac{\hbar e H k_x z}{mc} + \frac{(eHz)^2}{2mc^2} + U(z) - \varepsilon(k_x) \right] \varphi(k_x, z) = 0, \quad (3)$$

where the energy

$$\varepsilon(k_x) = \varepsilon_k - \frac{\hbar^2 k_y^2}{2m}.$$

It follows from Eq. (3) that for  $H \neq 0$  and an asymmetric potential  $U(z) \neq U(-z)$  there appears an asymmetric electron energy spectrum  $\varepsilon(k_x) \neq \varepsilon(-k_x)$ . To analyze the effect of interest to us, we shall employ a triangular quantizing model potential

$$U(z) = \begin{cases} \infty, & z < 0 \\ eEz, & z \geq 0 \end{cases} \quad (4)$$

employed for calculating the electron energy spectrum in inversion layers at semiconductor surfaces, where  $E$  is the electric field intensity at the surface.<sup>1</sup> Including in Eq. (3) a term  $\propto H^2$  gives corrections  $\sim (d/l_H)^4$  to the solution, where  $d$  is the characteristic thickness of the 2D layer and  $l_H = (\hbar c/eH)^{1/2}$  is the magnetic length. For many 2D systems  $d/l_H \ll 1$  in the entire range of magnetic fields realizable in practice, so that this term can be neglected. Then the solution of Eq. (3) with the potential (4) gives

$$\varepsilon(k_x) \approx \left[ \frac{\hbar^2}{2m} \right]^{1/3} \left[ \frac{3\pi}{2} \left( eE + \frac{\hbar e H k_x}{mc} \right) \left( n + \frac{3}{4} \right) \right]^{2/3} + \frac{\hbar^2 k_x^2}{2m}, \quad (5)$$

where  $n = 0, 1, 2, \dots$  is the number of the electronic subband in the 2D layer. Here  $\varphi(k_x, z)|_{z < 0} = 0$  and  $\varphi(k_x, z)|_{z \geq 0}$  is an Airy function:

$$\varphi(k_x, z) \approx \text{Ai} \left[ \left( \frac{2meE}{\hbar^2} + \frac{2eHk_x}{\hbar c} \right)^{1/3} \left( z - \frac{\varepsilon(k_x) - \hbar^2 k_x^2 / 2m}{eE + \hbar e H k_x / mc} \right) \right], \quad z \geq 0. \quad (6)$$

It follows from Eq. (5) that

$$\varepsilon(p_x) \neq \varepsilon(-p_x), \quad (7)$$

where  $p_x = (m_0/\hbar)[\partial\varepsilon(k_x)/\partial k_x]$  is the electron momentum along the  $x$  axis ( $m_0$  is the electron mass in vacuum and  $v_x = (1/\hbar)[\partial\varepsilon(k_x)/\partial k_x]$  is the electron velocity along the  $x$  axis). The physical reason for the appearance of the asymmetry (7) is as follows. A magnetic field parallel to the plane of the 2D system cannot induce a rotational motion of an electron along a cyclotron orbit and produces only a small change in the wave function. An electron moving with velocity  $v_x$  experiences a Lorentz force acting in the direction  $\langle -z \rangle$ , as a result of which the maximum of the electron wave function shifts in the direction  $\langle -z \rangle$ . For an electron moving with velocity  $-v_x$  the action of the Lorentz force is reversed and the maximum of the electron wave function shifts in the direction  $\langle z \rangle$ . For this reason, in an asymmetric potential  $U(z) \neq U(-z)$  the electron energy  $\varepsilon(v_x) \neq \varepsilon(-v_x)$ , which leads to Eq. (7). On account of the asymmetry (7), momentum transfer to the electron system in the presence of external perturbations is different for the directions  $\langle x \rangle$  and  $\langle -x \rangle$ . We shall demonstrate this effect for the specific example of the electron-photon interaction in an electron system with the energy spectrum (5).

Let an electromagnetic wave with frequency  $\omega$  and polarization vector  $\mathbf{e} \parallel \mathbf{z}$  propagate along the  $x$  axis. The vector potential  $\tilde{\mathbf{A}}$  of this wave has the form

$$\tilde{A}_z = A_0 \exp(-i\omega t) \exp(\pm iqx), \quad \tilde{A}_x = \tilde{A}_y = 0,$$

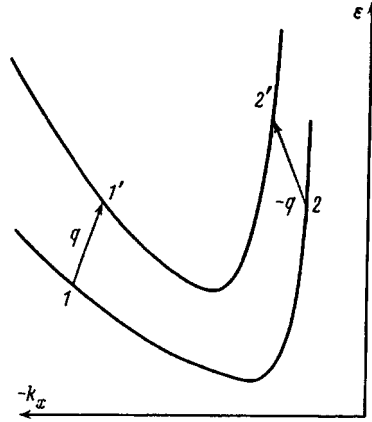


FIG. 1. Structure of intersubband electronic transitions accompanying the absorption of photons with wave vectors  $\mathbf{q}$  and  $-\mathbf{q}$ .

where  $\mathbf{q}$  is the wave vector and the  $\pm$  signs correspond to waves propagating in mutually opposite directions. Then the electron-photon interaction operator is

$$\hat{V} = \frac{e}{mc} \tilde{A}_z \hat{p}_z \quad (8)$$

and the probability that an electron absorbs a photon is

$$W = \sum_k \sum_{k'} \frac{1}{\hbar^2} |\langle \psi_{k'} | \hat{V} | \psi_k \rangle|^2 f(\varepsilon_k) [1 - f(\varepsilon_{k'})], \quad (9)$$

where  $f(\varepsilon_k)$  is the Fermi-Dirac distribution function. On absorbing a photon an electron passes from one subband (5) into another. The initial and final electron states  $k_x$  and  $k'_x$ , respectively, which satisfy the energy and wave vector conservation laws

$$\varepsilon(k'_{x1}) = \varepsilon(k_{x1}) + \hbar\omega, \quad k'_{x1} = k_{x1} + q, \quad \varepsilon(k'_{x2}) = \varepsilon(k_{x2}) + \hbar\omega, \quad k'_{x2} = k_{x2} - q, \quad (10)$$

are shown schematically in Fig. 1. Since the electronic subbands  $\varepsilon(k_x)$  are asymmetric for the directions  $\langle k_x \rangle$  and  $\langle -k_x \rangle$ , the wave functions  $\varphi(k_x, z)$  of the initial and final states of the electron change when the direction of the vector  $\mathbf{q}$  changes. It follows from Eqs. (10), (5), and (6) that  $\varphi(k_{x1}, z) \neq \varphi(k_{x2}, z)$  and  $\varphi(k'_{x1}, z) \neq \varphi(k'_{x2}, z)$ . Therefore the matrix element of the operator (8)

$$\langle \psi_{k'} | \hat{V} | \psi_k \rangle \propto \int_{-\infty}^{\infty} \varphi(k'_x, z) \frac{\partial \varphi(k_x, z)}{\partial z} dz$$

is different for the absorption of photons with vectors  $\mathbf{q}$  and  $-\mathbf{q}$ , on account of which the probabilities for the absorption of these photons are also different. Thus

$$W(\mathbf{q}) \neq W(-\mathbf{q}),$$

where

$$W(\mathbf{q}) = \frac{2\hbar}{\pi} \left( \frac{eA_0}{mc} \right)^2 J(k'_{x1}, k_{x1}) \quad (11)$$

is the absorption probability (9) per unit time and per unit area of a 2D system for a photon with wave vector  $\mathbf{q}$ , and

$$W(-\mathbf{q}) = \frac{2\hbar}{\pi} \left( \frac{eA_0}{mc} \right)^2 J(k'_{x2}, k_{x2}) \quad (12)$$

is the absorption probability (9) per unit time and per unit area of the 2D system for a photon with wave vector  $-\mathbf{q}$ . Here

$$\begin{aligned} J(k'_x, k_x) &= (|\varepsilon'(k'_x) - \varepsilon'(k_x)|)^{-1} \left( \int_{-\infty}^{\infty} |\varphi(k_x, z)|^2 dz \int_{-\infty}^{\infty} |\varphi(k'_x, z)|^2 dz \right)^{-1} \\ &\quad \times \int f \left( \varepsilon(k_x) + \frac{\hbar^2 k_y^2}{2m} \right) \left[ 1 - f \left( \varepsilon(k'_x) + \frac{\hbar^2 k_y^2}{2m} \right) \right] dk_y \\ &\quad \times \left( \int_{-\infty}^{\infty} \varphi(k'_x, z) \frac{\partial \varphi(k_x, z)}{\partial z} dz \right)^2, \end{aligned}$$

where

$$\varepsilon'(k) = \left. \frac{\partial \varepsilon(k_x)}{\partial k_x} \right|_{k_x=k},$$

and the integration over  $k_y$  extends over the first Brillouin zone.

We shall study the electron–photon interaction in the quantum limit (when all electrons occupy states in the subband (5) with  $n=0$ ) for the threshold intersubband absorption frequency  $\omega = \varepsilon_g/\hbar$  at temperature  $T=0$ ,  $k_F d_0 \sim 1$ , and  $H/E \ll 1$ , where  $\varepsilon_g$  is the energy gap between the subbands (5) with  $n=0$  and  $n=1$  for  $H=0$ ,  $k_F$  is the length of the Fermi wave vector of the electrons, and

$$d_0 = \left( \frac{3\hbar^2 \pi^2}{16meE} \right)^{1/3}$$

is the thickness of the 2D layer with  $H=0$ . In this case the photon absorption probabilities (11) and (12) assume the form

$$W(\mathbf{q}) = W_0 \left[ 1 - \frac{2}{3} \frac{H}{E} + O\left(\frac{H}{E}\right) \right], \quad (13)$$

$$W(-\mathbf{q}) = W_0 \left[ 1 + \frac{2}{3} \frac{H}{E} + O\left(\frac{H}{E}\right) \right], \quad (14)$$

where

$$W_0 = W(\mathbf{q})|_{H=0} = W(-\mathbf{q})|_{H=0}$$

is the probability of absorption of photons with wave vectors  $\mathbf{q}$  and  $-\mathbf{q}$  for  $H=0$ . We obtain from Eqs. (13) and (14) the anisotropy of the electron–photon interaction

$$\eta = \frac{W(-\mathbf{q}) - W(\mathbf{q})}{W_0} = \frac{4}{3} \frac{H}{E} + O\left(\frac{H}{E}\right). \quad (15)$$

Hence follows directly the anisotropy of momentum transfer: Identical electromagnetic waves propagating in opposite directions along the  $x$  axis are absorbed differently by electrons, as a result of which the momentum transfer from the electromagnetic waves to the electron system in the directions  $\langle x \rangle$  and  $\langle -x \rangle$  is different. Thus anisotropy of momentum transfer to electrons appears in the presence of a standing electromagnetic wave, acting as an isotropic (with respect to the directions  $\langle x \rangle$  and  $\langle -x \rangle$ ) external perturbation on the electron system, along the  $x$  axis. Anisotropic momentum transfer gives rise to an emf of photon drag of electrons in a standing electromagnetic wave. This is a new macroscopic quantum effect with no classical analogs. The magnitude of the emf is

$$\mathcal{E}_x = \frac{\hbar q L_x [W(-\mathbf{q}) - W(\mathbf{q})]}{e n_s}, \quad (16)$$

where  $n_s$  is the electron density per unit area of the 2D system and  $L_x$  is the length of the 2D system along the  $x$  axis. With consideration of Eq. (15), Eq. (16) assumes the form

$$\mathcal{E}_x / \mathcal{E}_{0x} = \eta,$$

where

$$\mathcal{E}_{0x} = \hbar q L_x W_0 / e n_s,$$

is the ordinary emf of photon drag of the electrons in a traveling electromagnetic wave with  $H=0$ . For  $H \sim 10^3$  G and  $d_0 \sim 10^{-7}$  cm we obtain  $\eta \sim 10^{-1}$ .

The asymmetry of the electron energy spectrum (7) that gives rise to the effect discussed above appears in the presence of a magnetic field not only in 2D systems but also in quasi-one-dimensional fullerene nanotubes with helical symmetry, on account of the asymmetry of such systems with respect to ‘‘clockwise’’ and ‘‘counterclockwise’’ rotations.<sup>2</sup> Therefore the electron–photon interaction in nanotubes<sup>3</sup> in the presence of a magnetic field directed along the axis of the tube will also be anisotropic: Electromagnetic waves propagating in opposite directions along the axis of a nanotube will be absorbed differently by the electrons.

The quite general discussions, which were based on conservation laws and led in the present work to the conclusion that the interaction of electrons with electromagnetic waves is anisotropic, also hold for the interaction of electrons with acoustic waves. Thus the phenomenon studied in this letter is universal.

<sup>a)</sup>e-mail: kibis@ref.nstu.nsk.su

<sup>1</sup>T. Ando, A. Fowler, and F. Stern, Rev. Mod. Phys. **54**, 437 (1982).

<sup>2</sup>D. A. Romanov and O. V. Kibis, Phys. Lett. A **178**, 335 (1993).

<sup>3</sup>O. V. Kibis and D. A. Romanov, *Fiz. Tverd. Tela (St. Petersburg)* **37**, 127 (1995) [*Sov. Phys. Solid State* **37**, 69 (1995)].

Translated by M. E. Alferieff

## Formation and magnetic properties of fractal aggregates of cobalt

I. V. Zolotukhin,<sup>a)</sup> A. B. Sukhodolov, and N. V. Tristan  
*Voronezh State Technical University, 394026 Voronezh, Russia*

A. S. Andreenko  
*M. V. Lomonosov Moscow State University, 119899 Moscow, Russian*

(Submitted 24 September 1997)

*Pis'ma Zh. Éksp. Teor. Fiz.* **66**, No. 8, 556–558 (25 October 1997)

Macroscopic fractal aggregates of cobalt are obtained by thermal evaporation of cobalt metal in an argon atmosphere and subsequent deposition on a silicon substrate heated to 1000 K. It is established that the fractal structure is formed by diffusion-limited aggregation of cobalt particles. The macroscopic fractal cobalt aggregates are ferromagnetic. © 1997 American Institute of Physics.

[S0021-3640(97)00920-1]

PACS numbers: 61.43.Hv, 75.50.Cc

Interest in condensed solids having a fractal structure has been increasing in recent years. Fractal structures of some substances (Fe, Zn, SiO<sub>2</sub>, MoO<sub>3</sub>, and NiCl<sub>2</sub>) have been obtained by aggregation of microscopic clusters produced by evaporation followed by cooling in a gaseous atmosphere.<sup>1–4</sup> The structure and physical properties of aggregates of this kind have essentially not been studied.

The objective of the present work was to develop a method for obtaining and to study the magnetic properties of fractal aggregates of cobalt. Cobalt was chosen for the following reasons. In discussing the mechanism leading to the formation of fractal clusters, a number of authors employ the model of diffusion-limited aggregation (DLA) for particles<sup>5</sup> and clusters<sup>6</sup> of the evaporated material. In Ref. 7, the ferromagnetic interaction of small cobalt particles was taken into account in an analysis of the formation of fractal aggregates of cobalt, but nothing was reported about the magnetic properties of structures of this kind. For this reason, we studied the problem of obtaining ferromagnetic fractal cobalt structures, clarifying the mechanism leading to the formation of such structures, and determining the magnetic properties.

Fractal aggregates of cobalt were obtained by thermal sputtering of atoms in an argon atmosphere followed by cooling of the condensation products on a polished silicon plate (the asperities did not exceed 10 nm in height). As shown in Ref. 4 and verified by us, fractal aggregates do not grow when asperities whose height is equal to or greater than the cluster size are present on the substrate surface. A cobalt charge was heated to  $T=2000$  K in an alundum crucible in a vacuum chamber at pressure  $P=10^{-4}$  torr using a tungsten coil. The chamber was filled with argon to pressure 0.1 torr immediately before the cobalt melted. Varying the argon pressure from 0.1 to 10 torr did not produce any qualitative changes in the structures obtained. The substrate, heated to 1000 K, was



FIG. 1.

located 10 cm from the sputtering source. This was sufficient for cobalt clusters to form before they reached the substrate. The quite high substrate temperature promotes diffusion of cobalt clusters along the surface of the polished silicon plate.

The fractal cobalt structures obtained were investigated with optical and scanning electron microscopes. The fractal dimension  $D$  of the aggregates was determined from the formula

$$L = cDS^{D/2},$$

where  $c$  is a constant and  $L$  and  $S$  are, respectively, the perimeter and area of the fractal aggregate. The fractal dimension of the structures formed was determined by varying  $L$  and  $S$ .<sup>8</sup>

The process leading to the formation of fractal structures is qualitatively as follows. It is known that evaporation results in the formation of a vapor–gas medium consisting of atoms (or molecules) with a substantial fraction (up to several percent) of charged ions, which with rapid cooling in a buffer gas (argon) act as centers of condensation of liquid clusters 10–30 nm in size.<sup>9</sup> After crystallization, the clusters continue to grow in size (according to the laws governing the formation of dust particles<sup>10</sup>) and reach 0.1–0.5  $\mu\text{m}$  in size before reaching the substrate. As a result of the high substrate temperature, the clusters intensively diffuse along the substrate surface and start to self-organize, forming star-shaped fractal aggregates consisting of self-similar branching structures ranging in

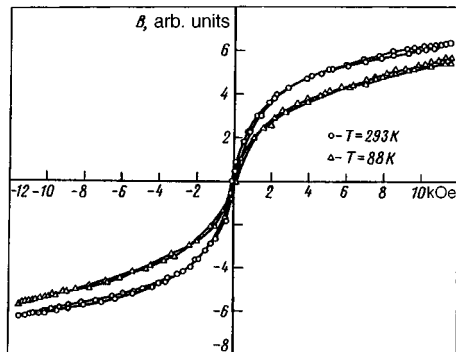


FIG. 2.

size from several microns to several millimeters (Fig. 1). Therefore, fractal aggregates of cobalt form by the DLA mechanism, made possible by the high mobility of clusters on the substrate heated to 1000 K. It should also be noted that individual fractal branches and undeveloped star-shaped structures are observed to grow at the edge of the substrate, where the concentration of the clusters reaching the substrate is lower than in the central part. Star-shaped aggregates with a branched structure form at the center of the substrate. The fractal dimension of the aggregates also varies from 1.2 to 1.7 from the edge to the center of the substrate, respectively.

The magnetization results for fractal aggregates of cobalt at 88 and 293 K are presented in Fig. 2 (curves 1 and 2). A characteristic feature of the magnetization curves for fractal aggregates of cobalt is that there is no saturation in external magnetic fields with intensity  $H$  up to 12 kOe, while ordinary cobalt samples saturate in fields  $H$  not exceeding 10 Oe. We believe that the magnetization difficulties are due to magnetic anisotropy, which arises during the formation of fractal structures, and the effect of the asperities on the surface of the aggregates on the magnetization reversal process. The coercive force is  $H_c \sim 105$  Oe for both the fractal and initial cobalt. According to published data, the values of  $H_c$  for cobalt range from 9 to 166 Oe depending on the structural state.<sup>11,12</sup>

In summary, the fractal aggregates of cobalt obtained are macroscopic (up to 2 mm) branched ferromagnetic structures formed by DLA. The coercive force of these structures is the same as for crystalline cobalt. However, in contrast to crystalline cobalt, the magnetization curves for fractal aggregates do not saturate in external magnetic fields up to 12 kOe.

<sup>a)</sup>e-mail: paul@zolut.vrn.ru

<sup>1</sup>S. R. Forrest and T. A. Witten, *J. Phys. A: Math. Gen.* **12**, L109 (1979).

<sup>2</sup>J. Z. Zhang and D. Liu, *J. Materials Science* **27**, 4329 (1992).

<sup>3</sup>J. Z. Zhang, *Phys. Rev. B* **41**, 9614 (1990).

<sup>4</sup>J. Z. Zhang *et al.*, *J. Phys.: Condens. Matter* **4**, L245 (1992).

<sup>5</sup>T. A. Witten and L. M. Sander, *Phys. Rev. Lett.* **47**, 1400 (1981).

- <sup>6</sup>P. Meakin, Phys. Rev. Lett. **51**, 1119 (1983).  
<sup>7</sup>G. A. Niclasson *et al.*, Phys. Rev. Lett. **60**, 1735 (1988).  
<sup>8</sup>J. M. Gomez-Rodriguez *et al.*, J. Phys. Chem. **96**, 347 (1992).  
<sup>9</sup>E. F. Mikhailov and S. S. Vlasenko, Usp. Fiz. Nauk **165**, 263 (1995).  
<sup>10</sup>V. N. Tsytoich, Usp. Fiz. Nauk **167**, 57 (1997).  
<sup>11</sup>R. M. Bozorth, *Ferromagnetism*, Van Nostrand, New York, 1951 [Russian translation, IL, Moscow, 1956].  
<sup>12</sup>L. F. Il'yushenko, *Electrolytically Deposited Magnetic Films* [in Russian], Nauka, Moscow

Translated by M. E. Alferieff

# Bose–Einstein condensation of an ideal gas in a parabolic trap

V. A. Alekseev,<sup>a)</sup> V. V. Klimov,<sup>b)</sup> and D. D. Krylova

*P. N. Lebedev Physical Institute, Russian Academy of Sciences, 117924 Moscow, Russia*

(Submitted 22 July 1997; resubmitted 15 September 1997)

*Pis'ma Zh. Éksp. Teor. Fiz.* **66**, No. 8, 559–563 (25 October 1997)

The temperature-dependent velocity distribution function is found for the case of Bose–Einstein condensation of a finite number of noninteracting atoms trapped in a three-dimensional anisotropic parabolic trap. It is shown that at a temperature  $T$  of the order of the condensation temperature  $T_0$  the velocity distribution consists of an anisotropic part, reflecting the population of the ground state, and an isotropic part above the condensate. © 1997 American Institute of Physics. [S0021-3640(97)01020-7]

PACS numbers: 03.75.Fi

In all experimental attempts made in the last two years to obtain a condensed state of a neutral Bose gas, the atoms were confined in traps with different configurations,<sup>1–3</sup> the condensation criterion being the appearance of anisotropy in the particle velocity distribution.<sup>1</sup> Nonetheless, the appearance of this anisotropy has still not been substantiated by a quantum-mechanical calculation. In the present letter, an exact quantum description of oscillator motion is used to calculate the single-particle velocity distribution function  $W(\mathbf{v})$  of an ideal gas confined by the potential  $V(\mathbf{r}) = \sum_i (m \omega_i^2 x_i^2 / 2)$  ( $T$  is the temperature and  $m$  is the mass of the atoms), which is a good approximation for well any real trap.

The chemical potential  $\bar{\mu} = \mu/T$  of the gas is determined by the equation

$$N = \sum_{k_x, k_y, k_z=0} (e^{\vec{\beta} \cdot \mathbf{k} - \bar{\mu}} - 1)^{-1}, \quad (1)$$

where  $N$  is the total number of particles,  $\beta_i = \hbar \omega_i / T$ ,  $i = x, y, z$ , and the energy of the oscillators is measured from the value  $2^{-1} \hbar (\omega_x + \omega_y + \omega_z)$ . Representing each term in the sum in Eq. (1) in the form

$$(e^{\vec{\beta} \cdot \mathbf{k} - \bar{\mu}} - 1)^{-1} = \sum_{s=1}^{\infty} \exp(s(-\vec{\beta} \cdot \mathbf{k} + \bar{\mu})) \quad (2)$$

and carrying out the summation over  $k_i$ , we obtain

$$N = \sum_{s=1}^{\infty} e^{\bar{\mu}s} \prod_{i=1}^3 (1 - e^{-\beta_i s})^{-1}. \quad (3)$$

In Ref. 4 the sum (3) is written in an integral form, which makes it possible to investigate all limiting cases. To calculate the velocity distribution function, we must obtain asymptotic expressions for the chemical potential directly from Eq. (3). It is convenient to rewrite the relation (3) in the form

$$N = \sum_{s=1}^{\infty} e^{\bar{\mu}s} + \sum_{s=1}^{\infty} e^{\bar{\mu}s} \left( \prod_{i=1}^3 (1 - e^{-\beta_i s})^{-1} - 1 \right). \quad (4)$$

The first sum equals the number of particles  $N_0 = (e^{-\bar{\mu}} - 1)^{-1}$  in the ground state and the second sum equals the number of particles in the excited states and remains convergent even after the factor  $e^{\bar{\mu}s}$  is dropped. For large  $\beta \gg 1$  (low temperatures) we obtain from Eq. (4)

$$N = (e^{-\bar{\mu}} - 1)^{-1} + \sum_i \exp(-\beta_i), \quad \bar{\mu} \approx -\frac{1}{N}, \quad N_0 \approx N. \quad (5)$$

As  $T$  increases, the  $\beta_i$  decrease. For small  $\beta \ll 1$  expression (4) can be written in the form

$$N = \frac{1}{e^{-\bar{\mu}} - 1} + \frac{1}{\beta_x \beta_y \beta_z} \sum_{s=1}^{\infty} e^{\bar{\mu}s} \frac{1}{s^3}, \quad \beta \ll 1, \quad (6)$$

and expression (6) is applicable for both small and large values of  $|\bar{\mu}|$ . For small  $|\bar{\mu}|$  we find from Eq. (6)

$$N = -\frac{1}{\bar{\mu}} + \left( \frac{T}{\hbar \bar{\omega}} \right)^3, \quad |\bar{\mu}| = N^{-1} \left( 1 - \left( \frac{T}{T_0} \right)^3 \right)^{-1}, \quad |\bar{\mu}| \ll 1, \quad (7)$$

where  $\bar{\omega} = (\omega_x \omega_y \omega_z / \zeta(3))^{1/3}$ ,  $\zeta(x)$  is the Riemann zeta function,  $\zeta(3) = \sum_{s=1}^{\infty} (1/s^3) \approx 1.2$ , and a condensation temperature  $T_0 = N^{1/3} \hbar \bar{\omega}$  is introduced by analogy to the quasiclassical approximation.<sup>5</sup> This expression also gives (see Eq. (5)) the correct value  $\bar{\mu} = -1/N$  in the limit  $T \rightarrow 0$ , but  $\bar{\mu}$  does not approach the limit in the correct manner. It is obvious from Eq. (7) that the absolute value  $|\bar{\mu}|$  becomes much less than 1 when  $N(\hbar \bar{\omega}/T)^3 = (T_0/T)^3 \gg 1$ , which for sufficiently large  $N$  is reached in the case  $\hbar \bar{\omega}/T \ll 1$ , i.e., in the region where Eq. (6) is applicable. As the temperature increases further,  $|\bar{\mu}|$  increases and for  $|\bar{\mu}| \gg 1$  we obtain from Eq. (6) an expression for  $\bar{\mu}$

$$N = e^{\bar{\mu}} \left( \frac{T}{\hbar \bar{\omega}} \right)^3 \zeta^{-1}(3), \quad \bar{\mu} = -\ln \left( \frac{1}{\zeta(3)} \left( \frac{T}{T_0} \right)^3 \right), \quad (8)$$

that is applicable at high temperatures  $N(\hbar \bar{\omega}/T)^3 = (T_0/T)^3 \ll 1$ . The population of the ground state decreases with increasing temperature:  $N_0 = \zeta(3)(T_0/T)^3$ . Figure 1 shows the results of the numerical solution of Eq. (1) and the temperature dependence obtained for  $|\bar{\mu}|$  and  $N_0$  from Eqs. (7) and (8) in the case of the potential employed in Ref. 1. The difference between Eq. (7) and Eq. (5) cannot be discerned in the figure.

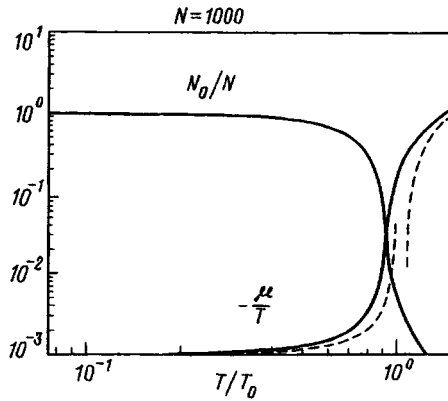


FIG. 1. Chemical potential  $-\mu/T$  versus temperature. Dashed curves — asymptotic functions (7) and (8) ( $N=1000$ ,  $\omega_x:\omega_y:\omega_z=1:1:2\sqrt{2}$ ).

To find the particle velocity distribution function  $W(\vec{\nu})$  let us examine the diagonal matrix element of the operator  $F = \sum_{\alpha} \delta(\nu - \nu_{\alpha})$  (summation over particles) for a wave function in the  $\vec{\nu} = \mathbf{p}/m$  representation with the occupation numbers  $N_0 N_1 \dots N_q$  (Ref. 6):

$$\langle N_0 N_1 \dots | F | N_0 N_1 \dots \rangle = N_0 |\Psi_0(\vec{\nu})|^2 + N_1 |\Psi_1(\vec{\nu})|^2 + \dots$$

The velocity distribution function is obtained by premultiplying this quantity by the probability  $\sigma(N_0 N_1 \dots) = Z \exp(-(\epsilon_0 N_0 + \epsilon_1 N_1 + \dots)/T)$  ( $Z$  is the partition function and  $\epsilon_i$  is the energy of the  $i$ th state) of being in the state  $|N_0 N_1 \dots\rangle$  and summing over all possible values of  $N_0, N_1, \dots$  under the condition  $N_0 + N_1 + \dots = N$  (Ref. 7):

$$\begin{aligned} W(\vec{\nu}) &= \sum_{N_0 N_1 \dots} \sigma(N_0 N_1 \dots) [N_0 |\Psi_0(\vec{\nu})|^2 + N_1 |\Psi_1(\vec{\nu})|^2 + \dots] \\ &= \sum_n \langle N_n \rangle |\Psi_n(\vec{\nu})|^2, \end{aligned} \quad (9)$$

where  $\langle N_n \rangle = (\exp((\epsilon_n - \mu)/T) - 1)^{-1}$  is the average number of particles on the  $n$ th level. Next, using expression (2) we obtain from Eq. (9)

$$W(\mathbf{p}) = \sum_{s=1}^{\infty} e^{s\bar{\mu}} \bar{G}(\mathbf{p}, \mathbf{p}, \eta s). \quad (10)$$

Here  $\eta = 1/T$ , and  $\bar{G}(\mathbf{p}, \mathbf{p}', \eta s)$  is the Green's function (instantaneous point source function<sup>8</sup>) in the momentum representation:

$$\bar{G}(\mathbf{p}, \mathbf{p}', \eta) = \sum_n e^{-E_n \eta} \Psi_n(\mathbf{p}) \Psi_n(\mathbf{p}'), \quad (11)$$

which can be obtained by Fourier transforming the Green's function in the coordinate representation

$$\bar{G}(\mathbf{r}, \mathbf{r}', \eta) = \sum_n e^{-E_n \eta} \Psi_n(\mathbf{r}) \Psi_n(\mathbf{r}'), \quad \hat{H} \Psi_n(\mathbf{r}) = E_n \Psi_n(\mathbf{r}), \quad (12)$$

which satisfies the Schrödinger equation with imaginary time

$$\frac{\partial \bar{G}(\mathbf{r}, \mathbf{r}', \eta - \eta')}{\partial \eta} + \hat{H} \bar{G} = \delta(\mathbf{r} - \mathbf{r}') \delta(\eta - \eta'). \quad (13)$$

In the oscillator case  $\epsilon_n/T = \epsilon_{\mathbf{k}}/T = \vec{\beta} \cdot \mathbf{k}$ , and we obtain from Eq. (9)

$$W(\vec{\nu}) = \sum_{k_x, k_y, k_z=0}^{\infty} (e^{\vec{\beta} \cdot \mathbf{k} - \bar{\mu}} - 1)^{-1} \Psi_{k_x}^2(\nu_x) \Psi_{k_y}^2(\nu_y) \Psi_{k_z}^2(\nu_z), \quad (14)$$

where

$$\Psi_k(\nu) = \left( \frac{\sqrt{q_k}}{\sqrt{\pi 2^n n!}} \right)^{1/2} \exp\left(-\frac{1}{2} q_k \nu^2\right) H_k(\sqrt{q_k} \nu), \quad q_k = \frac{m}{\hbar \omega_k}.$$

Using Eq. (2) once again, we perform the summation over the indices  $k_i$  and find

$$W(\vec{\nu}) = \sum_{s=1}^{\infty} e^{\bar{\mu}s} \prod_{i=1}^3 G(\nu_i, q_i, \beta_i s), \quad (15)$$

where  $G$  is a Bloch function<sup>7</sup>

$$G(\nu, q, \beta) = \sqrt{\frac{q}{\pi}} (1 - e^{-2\beta})^{-1/2} \exp\left(-q \nu^2 \tanh \frac{\beta}{2}\right),$$

where, as one can see from Eq. (3),  $\int W(\vec{\nu}) d\vec{\nu} = N$ .

For  $\beta_i \gg 1$ , we obtain from Eq. (5)  $\bar{\mu} = -1/N$  and expression (15) assumes the form

$$W(\vec{\nu}) = N \Psi_0^2(\vec{\nu}) = N \prod_{i=1}^3 \sqrt{\frac{m}{\pi \hbar \omega_i}} \exp\left(-\frac{m \nu_i^2}{\hbar \omega_i}\right), \quad (16)$$

reflecting the fact that all particles are in the ground state. If the frequencies  $\omega_i$  are all different, this function is anisotropic. At high temperatures, when  $|\bar{\mu}| \gg 1$  and  $\beta_i = \hbar \omega_i/T \ll 1$ , Eqs. (14) and (15) give an isotropic Maxwellian distribution corresponding to temperature  $T$ .

The most interesting region is the transitional region, where the condition  $\beta \ll 1$  is still satisfied but  $|\bar{\mu}|$  becomes small,  $|\bar{\mu}| \ll 1$ . As one can see from Eq. (7), this holds, for example, for  $\bar{\mu} = -2/N$  and  $\beta_i = \beta = (N/2.4)^{-1/3}$  so that for  $N=2400$  we have  $\beta = \hbar \bar{\omega}/kT = 0.1$  (we note that in this case  $\bar{\mu} \ll \beta$ ). To investigate this case it is convenient to rewrite Eq. (15) in the form

$$W(\vec{\nu}) = \frac{\Psi_0^2(\vec{\nu})}{e^{-\bar{\mu}} - 1} + \sum_{s=1}^{\infty} e^{\bar{\mu}s} \left( \prod_{i=1}^3 G(\nu_i, q_i, \beta_i s) - \Psi_0^2(\vec{\nu}) \right), \quad (17)$$

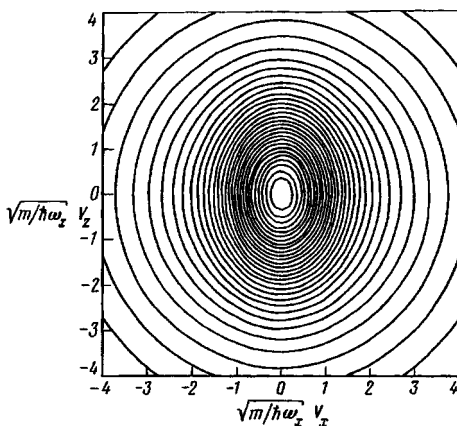


FIG. 2. Isolines of the single-particle distribution function (17) near the transition point ( $N=1000$ ,  $\omega_x:\omega_y:\omega_z=1:1:2\sqrt{2}$ ,  $T=1.16T_0$ ).

for which the series over  $s$  converges even after the factor  $e^{\bar{\mu}s}$  is dropped. We note that for the example presented above, one-half the total number of particles corresponds to each of the terms in Eq. (17). Expanding the exponential  $e^{-\beta_i s}$  in the arguments of  $G$  and dropping in the second term the function  $\Psi_0^2(\vec{\nu})$ , whose contribution is small, we obtain

$$W(\vec{\nu}) = -\frac{\Psi_0^2(\vec{\nu})}{\bar{\mu}} + L(\vec{\nu}), \quad L(\vec{\nu}) = \left(\frac{m}{2\pi}\right)^{3/2} \frac{T^{3/2}}{\hbar^3 \bar{\omega}^3 \zeta(3)} \sum_{s=1}^{\infty} \exp\left(-\frac{m\vec{\nu}^2}{2T}s\right) \frac{1}{s^{3/2}}. \quad (18)$$

In contrast to  $\Psi_0^2(\vec{\nu})$ , the distribution  $L(\vec{\nu})$  is always spherically symmetric and, as was indicated in Ref. 1, the presence of these two terms is the main evidence for Bose-Einstein condensation. The sum in Eq. (18) can be represented in the form

$$\sum_{s=1}^{\infty} \exp\left(-\frac{m\nu^2}{2T}s\right) \frac{1}{s^{3/2}} = \exp\left(-\frac{m\nu^2}{2T}\right) \varphi\left(\frac{m\nu^2}{2T}\right), \quad \varphi(\xi) = \frac{2}{\sqrt{\pi}} \int_0^{\infty} \frac{\sqrt{t} dt}{e^t - e^{-\xi}}. \quad (19)$$

The function  $\varphi(\xi)$  decreases with increasing  $\xi$  from  $\varphi(0) = \zeta(3/2) \approx 2.6$  to  $\varphi(\infty) = 1$ ; interestingly,  $\varphi'(0) = \infty$ . Hence it follows that  $L(\vec{\nu})$  has a characteristic width  $\nu \sim \sqrt{T/m} = \sqrt{\hbar\bar{\omega}/\beta m} \gg \sqrt{\hbar\bar{\omega}/m}$ , where  $\sqrt{\hbar\bar{\omega}/m}$  is the width of the function  $\Psi_0^2(\vec{\nu})$ , and a diffuse peak at  $\nu=0$ . Isolines and the three-dimensional form of the distribution function (17) near the transition point are shown in Figs. 2 and 3, whence the anisotropic part (at the center) and the isotropic part (at the periphery) are clearly seen.

Integrating expression (18) over the velocities, we obtain the relation (7). This confirms the correctness of the procedure performed.

We recall that Eqs. (7) and (18) are applicable when, generally speaking, the contradictory conditions  $|\bar{\mu}| \ll 1$ ,  $N(T/T_0)^3 \sim 1/\beta^3 \gg 1$  are satisfied. However, it is evident from Eq. (7) that for large  $N \sim 10^3$ ,  $|\bar{\mu}|$  remains small all the way up to very large values

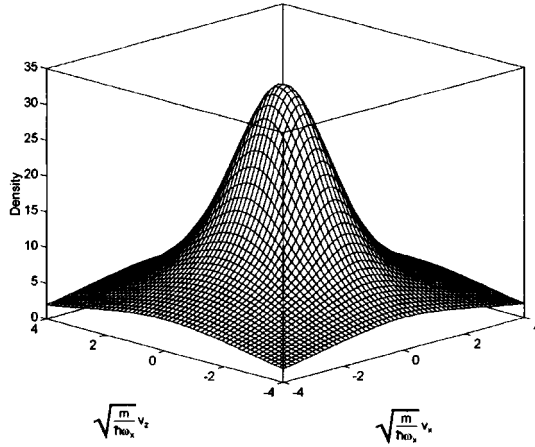


FIG. 3. Three-dimensional form of the single-particle distribution function (17) near the transition point ( $N=1000$ ,  $\omega_x:\omega_y:\omega_z=1:1:2\sqrt{2}$ ,  $T=1.16T_0$ ).

of  $N(T/T_0)^3$ ; for example,  $|\bar{\mu}| < 0.1$  up to values  $(T/T_0)^3 < 1 - 10/N \approx 1$ . This means that the condensation proceeds as follows (see Fig. 1). For  $(T/T_0)^3 > 1$ ,  $|\bar{\mu}| > 1$  and Eqs. (14) and (15) give the standard Maxwellian distribution. As the temperature decreases, condensation starts when  $1/N < (T/T_0)^3 < 1$  (Eq. (18)). The number of condensed particles with, generally speaking, an anisotropic distribution function  $\Psi_0^2(\vec{\nu})$  equals  $N(1 - (T/T_0)^3)$ , while  $N(T/T_0)^3$  particles are in the ordinary fraction with a wide distribution. This process lasts, for example, down to  $N(T/T_0)^3 = 10$ , when there are  $N - 10$  particles in the condensed fraction. As the temperature decreases further,  $N(T/T_0)^3 \leq 1$ , in accordance with Eq. (5) condensation accelerates and all particles drop into the lower oscillator level with distribution function  $\Psi_0^2(\vec{\nu})$ .

Expressing the temperature  $T_0$  in terms of the volume  $V$  occupied by the gas,  $m\omega^2 x^2 \sim T_0$ ,  $V \sim x^3 \sim 1/\omega^3 (T_0/m)^{3/2}$ , we find that to within a numerical factor  $T_0$  equals the temperature  $T_0$  for a gas of free particles.<sup>9</sup>

This work was supported in part by the Russian Fund for Fundamental Research under Grants Nos. 96-02-18695 and 96-02-19753 (V. V. K.) and the State Science and Technology Program "Metrology."

<sup>a)</sup>e-mail: valeks@sci.lebedev.ru

<sup>b)</sup>e-mail: klimov@rim.phys.msu.su

<sup>1</sup>M. H. Anderson, J. R. Ensher, M. R. Matthews *et al.*, *Science* **269**, 198 (1995).

<sup>2</sup>C. C. Bradley, C. A. Sackett, J. J. Tolett *et al.*, *Phys. Rev. Lett.* **75**, 1687 (1995).

<sup>3</sup>K. B. Davis, M.-O. Mewes, M. R. Andrews *et al.*, *Phys. Rev. Lett.* **75**, 3969 (1995).

<sup>4</sup>K. Kirsten and D. J. Toms, *Phys. Rev. A* **54**, 4188 (1996).

<sup>5</sup>V. Bagnato, D. E. Pritchard, and D. Kleppner, *Phys. Rev. A* **35**, 4354 (1987).

<sup>6</sup>L. D. Landau and E. M. Lifshitz, *Quantum Mechanics*, 3rd ed., Pergamon Press, New York, 1977 [cited Russian original, Nauka, Moscow, 1989].

<sup>7</sup>M. A. Leontovich, *Introduction to Thermodynamics. Statistical Physics* [in Russian], Nauka, Moscow, 1983.

<sup>8</sup>R. Feynman, *Statistical Mechanics: A Set of Lectures*, Benjamin, Reading, Mass., 1972 [Russian translation, Mir, Moscow].

<sup>9</sup>L. D. Landau and E. M. Lifshitz, *Statistical Physics*, Pergamon Press, New York [Russian original, Nauka, Moscow, 1995, Part 1].

Translated by M. E. Alferieff